STRUCTURAL SETTING AND METAMORPHIC EVOLUTION OF A CONTACT AUREOLE: THE EXAMPLE OF THE MT. CAPANNE PLUTON (ELBA ISLAND, TUSCANY, ITALY)

Enrico Pandeli*,°,✉, **Riccardo Giusti***, **Franco Marco Elter****, **Andrea Orlando**° and **Letizia Orti***

* *Department of Earth Sciences, University of Florence, Italy.*
** *DISTAV, University of Genoa, Italy.*
° *CNR-Institute of Geosciences and Earth Resources, U.O.S. of Florence, Italy.*
✉ *Corresponding author, email: enrico.pandeli@unifi.it*

Keywords: *contact metamorphism, plutonism, structural geology, Ligurids. Elba Island, Italy.*

ABSTRACT

This paper shows an updated geological, petrographical-chemical and structural picture of the contact aureole of the 6.9 Ma Mt. Capanne monzogranitic pluton in western Elba Island (Tuscan Archipelago), that is one of the most known Tertiary intrusive bodies in Italy. Most of the foliated metamorphic rocks derived from a Mesozoic Ligurian-type ophiolitic succession (Punta Polveraia-Fetovaia Unit) and are in the horneblende to pyroxene hornfels facies with estimated Tpeak > 610°C (locally > 650°C). Local variations of the metamorphic zonation of the at least 150-200 m thick aureole are due to the different lithological, physical and structural (e.g., bedding, fracturing) nature of the original rocks, but also to hydrofracturing phenomena which occurred during the syn-metamorphic upflow of the metasomatic hot fluids. The history of the emplacement and uplift of the Mt. Capanne pluton was defined through the metamorphic-structural evolution of its contact metamorphic aureole. The growth of the thermometamorphic minerals took place in several stages being both syn-kinematic with respect to the main ductile D_2 folding event (connected to the plutonic intrusion) and static post-kinematic one. Ductile shear zones, characterized also by mylonites, were also active during recrystallization in a general shear-type regime (average value of $W_m = 0.7$) related to the vertical uplift of the pluton (pure shear) and lateral ductile flow of the covers (simple shear). The exhumation of the cooled pluton continued producing tangential cascade-type folding event (D_3), detachment faults, and later high-angle faulting in the host rocks. The role of Western Elba in the geological frame of the whole island since Late Miocene times is also outlined in the paper.

INTRODUCTION

The Elba Island is located in the Tuscan Archipelago (Northern Tyrrhenian Sea) between the Northern Apennines (including Tuscany) and the Corsica Alpine Orogenic belts (Fig. 1). This island is wellknown not only for its iron ore bodies and for pegmatite and hydrothermal minerals (Tanelli et al., 2001), but also for its peculiar and complex tectonic building that was modified by the intrusion and ascent of Late Miocene acidic plutons that produced detachments and the final emplacement of the nappes (Pertusati et al., 1993; Bouillin et al., 1994; Daniel and Jolivet, 1995; Bortolotti et al., 2001a; 2001b; Principi et al., 2015a; 2015b and references therein). The granodioritic Mt. Capanne pluton is well exposed in western Elba as well as its contact metamorphic aureole. Previous papers dealt with: a) the mineralogy, petrography and petrology of the granitoid and its dike swarm (Marinelli, 1959; Westerman et al., 2004; Gagnevin et al., 2004; 2008; Farina et al., 2010; Rocchi et al., 2010; Poli and Peccerillo, 2016) including pegmatites (Orlandi and Pezzotta, 1997; Pezzotta 2000) b) geology and structural aspects of this plutonic system (Spohn, 1981; Reutter and Spohn, 1982; Bouillin. 1983; Boccaletti and Papini, 1989; Bouillin et al., 1993; 1994; Daniel and Jolivet, 1995; Perrin, 1975; Coli and Pandeli, 2001; Bortolotti et al., 2001b; Cifelli et al., 2012; Pandeli et al., 2013), c) the thermo-rheological model of the pluton (Caggianelli et al., 2013), d) the petrographic features of the thermal aureole and the circulation of magmatic-hydrothermal fluids in it (Marinelli, 1959; Barberi and Innocenti, 1965; 1966; Rossetti et al., 2007; Rossetti and Tecce, 2008). Few papers of these (Bouillin, 1983; Daniel and Jolivet, 1995; Rossetti et al., 2007) analyzed the relationships between the blastesis and deformation framework of the hornfels in some part of the aureole respect to the emplacement of the plutonic body.

In this study, we performed a comparative geological, petrographical- mineralogical (Electron microprobe and X-rays) and structural study extended to the whole aureole for obtaining an updated evolutive model of the host rocks during the magmatic intrusion and subsequent exhumation/uplift. The present paper aims at showing the first results of these studies and the refinement of the evolutive scheme of the Elba Island evolution since Tortonian times.

GEOLOGICAL OUTLINE OF THE ELBA ISLAND

The geological frame of the Elba Island is very peculiar and complex because it was controlled not only by the Alpine compressional and extensional orogenic phases, but also by the emplacement of the Late Miocene magmatic bodies (Bortolotti et al., 2001a; 2001b; Principi et al., 2015a; 2015b and references therein).

The island can be divided into two parts, according to their geological and geomorphological features (Figs. 1 and 2): a) the central-eastern Elba, where the whole tectonic pile is well exposed and was intruded by the Porto Azzurro Quartz-monzonite in its lower portion; b) the western Elba, dominated by the Mt. Capanne (1019 m) granodioritic stock with its contact metamorphic ~~aureole; b).~~

The tectonic pile of Elba Island includes Tuscan Units (derived from the Paleozoic to Tertiary Adria paleo-continental margin) and Ligurian and Ligurian-Piedmontese Units (derived from Jurassic to Eocene paleo-oceanic domains). Barberi et al. (1969a; 1969b) distinguished five thrust complexes: three Tuscan Units (Complexes I, II and

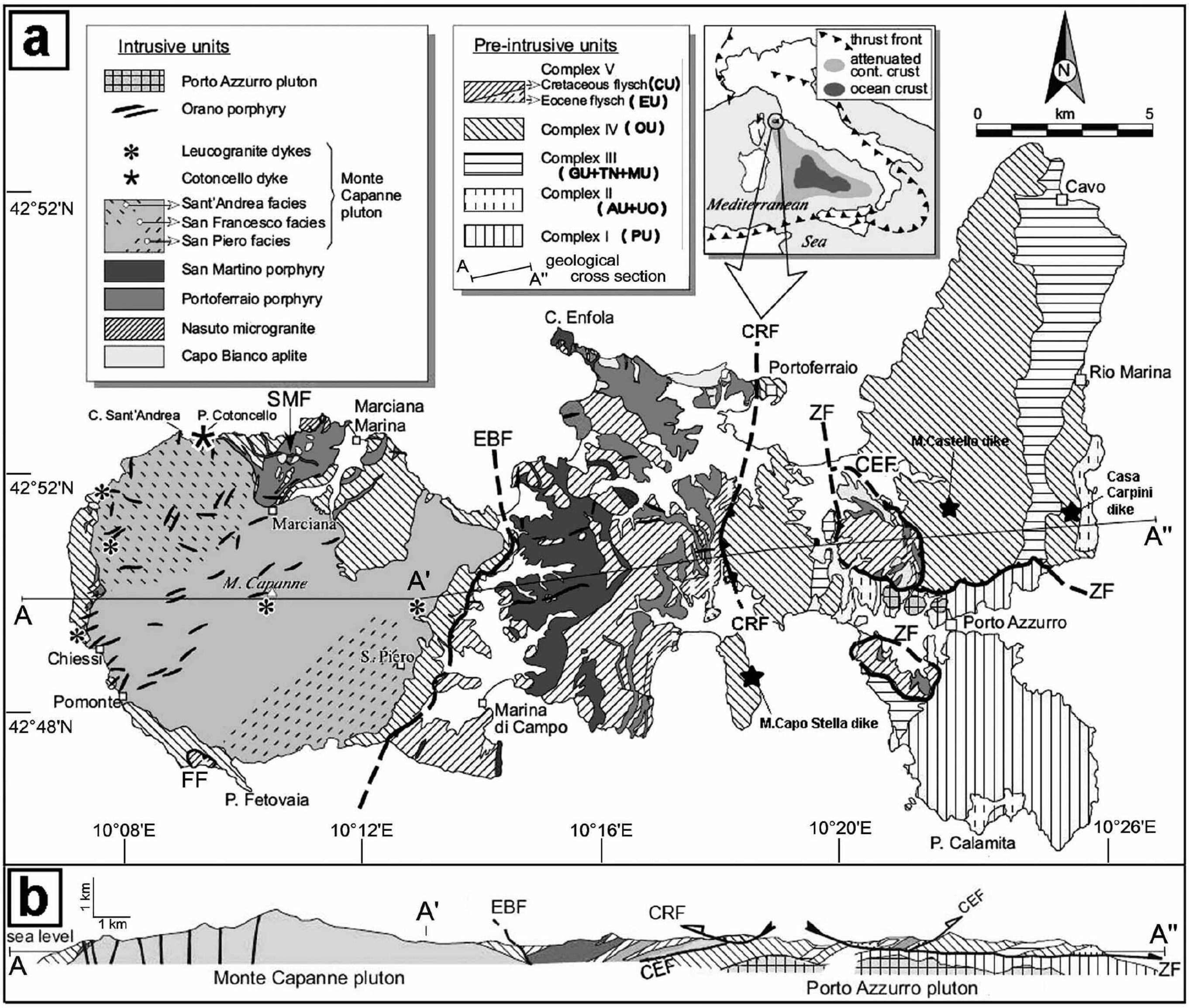

Fig. 1 - Geological map (a) and section (b) of the Elba Island, including the different magmatic bodies (modified from Westerman et al., 2003). EBF- Eastern Border Fault (Colle Palombaia-Procchio Fault in this paper), CEF- Central Elba Fault, ZF- Zuccale Fault, CRF- Colle Reciso Fault, FF- Fetovaia Fault. The correspondence of the five Trevisan's (1950) Complexes with Bortolotti's et al. (2001a) Units is reported in the legend of the pre-intrusive Units: PU- Porto Azzurro Unit; UO- Ortano Unit; AU- Acquadolce Unit; MU- Monticiano-Roccastrada Unit; TN- Tuscan Nappe; GU- Gràssera Unit; OU- Monte Strega Unit; EU- Lacona Unit; CU- Ripanera Unit.

III) overlain by two Ligurian Units (Complexes IV and V) (Fig. 1). The upper four complexes lie directly on the substantially autochthonous Complex I. According to the new model of Principi et al. (2015a; 2015b; 2015c), nine main tectonic units were defined, from bottom to top of the structural stack (Figs. 1 and 2):

1- The Tuscan Porto Azzurro Unit (PU) is made up of mainly pelitic hornfelses (due to the recrystallization of the Porto Azzurro intrusion) after Paleozoic rocks including also Grt-bearing micaschists, ~~quartzites~~ and amphibolites (Mt. Calamita Complex) and overlying Triassic-Jurassic quartzites and marbles (Garfagnoli et al., 2005; Musumeci et al., 2010).

2- The Tuscan Ortano Unit (UO) includes Early Paleozoic acidic meta-volcanic and -volcanoclastic rocks and phyllitic-quartzitic metasediments (see also Musumeci et al., 2010).

3- The Acquadolce Unit (AU) is represented by a HP-LT metamorphic succession of marbles and calcschists grading upwards into metasiliciclastics with intercalations of Early Cretaceous calcschists and rare metabasite levels and a serpentinite slice is at the top (Duranti et al., 1992; Bianco et al., 2015). A 19 Ma $^{40}Ar/^{39}Ar$ age was defined on muscovite for the main folding event of AU (Deino et al., 1992). AU has been correlated to the HP-LT Ligurian-Piedmontese successions i.e "Schistes Lustrés" (Bortolotti et al., 2001b; Pandeli et al., 2001a) or to a Tuscan metamorphic succession (Barberi et al., 1969b; Bianco et al., 2015; Massa et al., 2016).

4- The Tuscan Monticiano-Roccastrada Unit (MU) includes Late Carboniferous-Early Permian to Late Triassic metasiliciclastic rocks and Jurassic to Oligocene epimetamorphic formations with a metamorphic peak dated about 30 Ma (zircon fission tracks in Balestrieri et al., 2011), 5- The unmetamorphic Tuscan Nappe (TN) is composed mainly of calcareous-dolomitic, at times vacuolar, breccias (Rioalbano Breccia, "Calcare Cavernoso" Auctt.) but, northwards of Rio Marina, they are overlain by carbonate, carbonate-siliceous and calcareous-marly formation of Late Triassic to Dogger age.

6- The Gràssera Unit (GU) mostly consists of varicoloured slates and of rare carbonate-siliceous and radiolarite intercalations, overlying a basal calcschist member. GU has been considered as a Ligurian-Piedmontese Unit (Bortolotti et al., 2001b; Pandeli et al., 2001b) or is included it in the Tuscan Nappe (Barberi et al., 1969a; 1969b; Massa et al., 2016).

7- The Ligurian Monte Strega Unit (OU) is made up of the Mesozoic oceanic succession of the Vara Unit cropping out in Liguria and Tuscany and consists of serpentinites, ophicalcites, Mg-gabbros and volcanic-sedimentary cover (from Basalts to Palombini Shales) (Barberi et al., 1969a; 1969b; Bortolotti et al., 1994a; 2001). Bortolotti et al. (2001a) divided OU into six tectonic subunits (Fig. 2; see also Fig. 22 in Principi et al., 2015b).

8- The Ligurian Lacona Unit (EU) is constituted by shales with calcareous-marly, calcarenitic and arenaceous intercalations and, locally, by nummulite-bearing ophiolitic breccias of Middle Eocene age.

9- The Ligurian Ripanera Unit (CU) is mostly represented by a Late Cretaceous, Helminthoid-type calcareous-marly-arenaceous torbiditic deposits.

In the western part of the Island, two main Ligurian ophiolitic units surround the Mt. Capanne pluton (Fig. 2a, b): 1) the thermometamorphosed Punta Polveraia-Fetovaia Unit i.e the contact metamorphic aureole of the pluton (PFU) (see details later) which tectonically underlies, through the Fetovaia Fault (FF in Figs. 1 and 2); 2) the unmetamorphic Punta Le Tombe Unit (PTU) that is a calcareous-marly-shaly, turbiditic succession of Paleocene-Eocene age including ophiolitic mono- and polymictic breccias, olistoliths and an olistostrome. PFU was related by Marinelli (1959), Barberi and Innocenti (1965; 1966) and Bouillin (1983) to OU of eastern Elba (i.e. OU), whereas other Authors (Perrin 1975; Spohn 1981; Reutter and Spohn 1982; Coli and Pandeli, 2001) referred them to Ligurian-Piedmontese "Schistes Lustrés". In this frame Perrin (1975) define the Alps-Apennine boundary as passing through central Elba. Instead, PTU can be easily correlated to EU of central-eastern Elba.

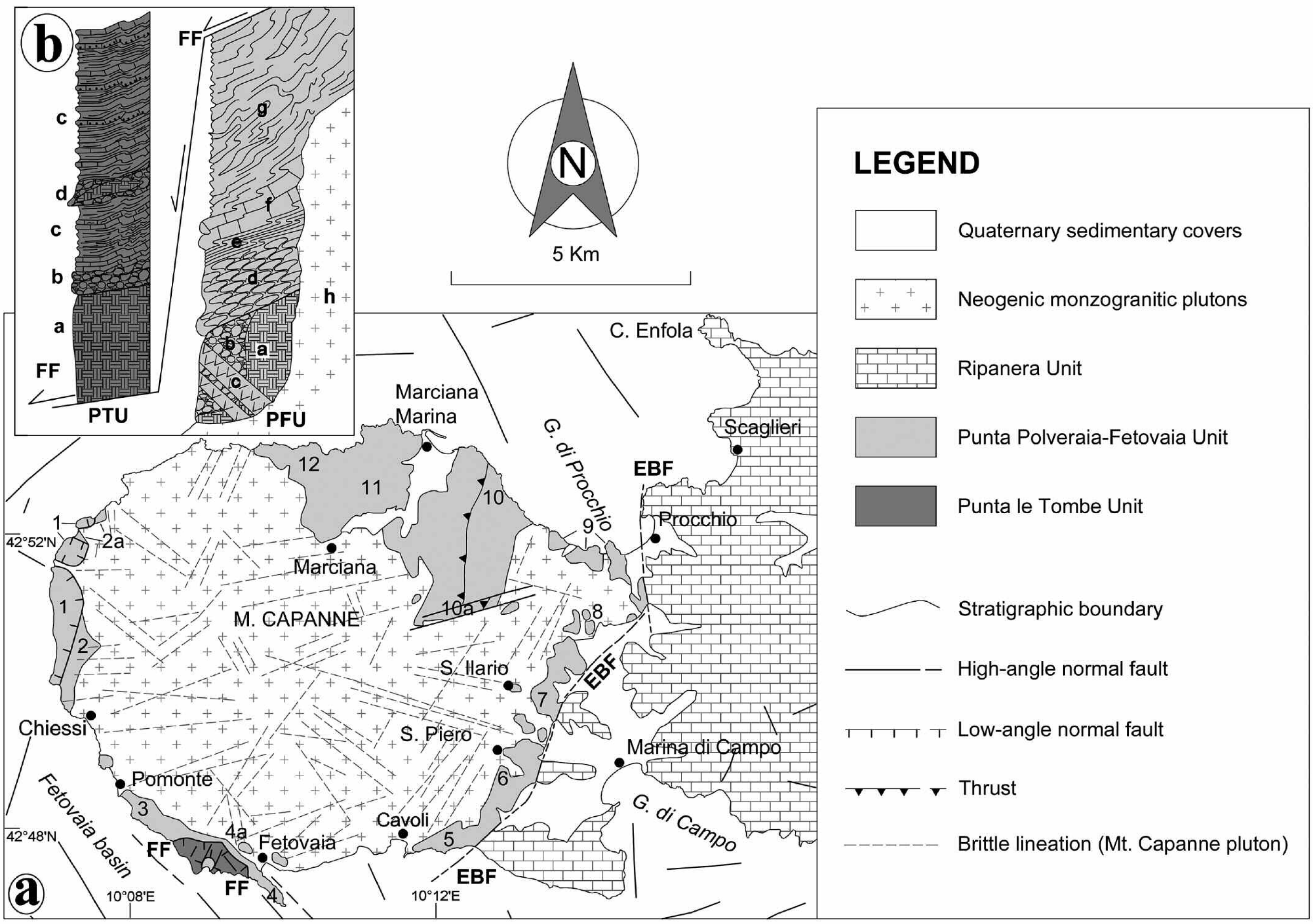

Fig. 2 - a) Tectonic scheme of Western Elba Island (modified from Principi et al., 2015a; 2015b) and location of the studied sites. EBF- Colle Palombaia-Procchio Fault, FF- Fetovaia Fault. Sampling sites: 1) Punta Nera-Punta Polveraia, 2) Punta del Timone-Il Semaforo, 2a) Beach between Punta Polveraia-Punta Fornace, 3) Pomonte-Fosso Ogliera, 4) Punta Fetovaia, 4a) Fetovaia, 5) Cavoli-Colle Palombaia, 6) San Piero, 7) Sant'Ilario, 8) Marmi, 9) Punta Sprizze-Spartaia -Punta dell'Agnone, 10) Bagno-Marciana Marina, 10a) Mt. Perone 11) Marciana-Marciana Marina, 12) Maciarello.
b) Structural-stratigraphic sketch of western Elba (the stratigraphic columns are not in scale): PFU- Punta Polveraia-Fetovaia Unit (a-serpentinites, b-metagabbros, c-basic metadikes, d- metabasalts, e-metacherts, f- metalimestones, g- metashales and metalimestones, h- Mt. Capanne Monzogranite), PTU- Punta Le Tombe Unit (a-serpentinites, b- Punta Le Tombe breccias and olistostrome, c- Mt. Agaciaccio limestones and marlstones; d- olistoliths and breccias).

According to most of the Authors (see Principi et al., 2015b and references therein), the structural framework of the Elba Island is characterized by an imbricate stack of structural units, separated by low-middle angle tectonic surfaces (thrusts and detachments), which lay onto the lowermost PU (= Trevisan's Complex I) by a main low-angle Zuccale Fault (= ZUC in Fig. 1). Some of these tectonic surfaces were reused in different times and in different tectonic regimes (e.g, inversion of the thrusts during the following extensional regime). According to many Authors (Pertusati et al., 1993; Bouillin et al., 1994; Bortolotti et al., 2001b; Maineri et al., 2003; Westerman et al., 2004; Garfagnoli et al., 2005; Principi et al., 2015a; 2015b), low-angle faulting and detachments occurred in the tectonic stack during the Late Miocene intrusion and exhumation of the two main plutons. First, the rise of the Mt. Capanne stock (intruded in PFU), produced the detachment of the uppermost units (the already piled CU and EU) and their main sliding to east through the Central Elba Fault (= CEF in Maineri et al., 2003; Principi et al., 2015a; 2015b) (Figs. 1 and 2). Similarly, the following intrusion of the Porto Azzurro Pluton within PU, allowed the detachment of the whole overlying pile of nappes, producing 1) the typical OU to CU embricate tectonic stack above PU through the main east-vergent ZUC and 2) the westward superimposition of UO above EU in central Elba through the Colle Reciso Fault (Principi et al., 2015a; 2015b) (= CRF, Figs. 1 and 2) (Principi et al., 2015a; 2015b and references therein). Finally SW-NE, WSW-NNE and N-S trending normal faulting occurred in both western (e.g., the Eastern Border Fault = EBF, Fig. 2) and, particularly, in eastern-central Elba and in Mt. Calamita Promontory. These structures, that cut the whole tectonic pile including ZUC, are filled by the 5.4 to 4.8 Ma hematite-rich mineralizations (U-Th-He and K/Ar ages on specularite and adularia, respectively in Lippolt et al., 1995) along the Terranera-Rio Marina-Mt. Calendozio alignment.

The magmatic framework of the island is mainly characterized by two main Messinian monzogranitic plutonic bodies along with their micro- to leuco-granite, aplite and pegmatite dike swarms in western (Mt. Capanne pluton) and eastern (Porto Azzurro pluton) Elba Island (Marinelli 1959; Boccaletti and Papini, 1989; Rocchi et al., 2002; Dini et al., 2002; 2008a; 2009; Westerman et al., 2003; 2004; Poli 1992; Farina et al., 2010; Rocchi et al., 2010; Barboni and Schoene, 2014; Poli and Peccerillo, 2016) (Figs. 1 and 2) that are referred to the Tuscan Magmatic Province (Serri et al., 1993; Poli and Peccerillo, 2016 and references therein). A lot of radiometric ages using K/Ar, Rb/Sr, U-Pb and $^{40}Ar/^{39}Ar$ methods were obtained for the different magmatic bodies cropping out in the island during the last forty years (Saupé et al., 1982; Juteau et al., 1984; Ferrara and Tonarini, 1985; 1993; Dini et al., 2002; Maineri et al., 2003; Musumeci et al., 2010 and references therein).

The magmatic activity in the island began with the emplacement between ~ 8.3 and 7.4 Ma (using K/Ar on biotite, Rb/Sr on muscovite, biotite and feldspars, and $^{40}Ar/^{39}Ar$ on muscovite radiometric methods) of a "Christmas-tree"-type subvolcanic multilayer laccolithic-dike complex, including four intrusive units (Punta del Nasuto Microgranite, Capo Bianco Aplite, Portoferraio Porphyry and San Martino Porphyry: Dini et al., 2002; Rocchi et al., 2002; 2010). This complex intruded the ophiolitic successions around Mt. Capanne (PFU) and CU and EU now present in central-eastern Elba (see Fig. 3 in Rocchi et al., 2010).

The younger Mt. Capanne pluton (6.9 Ma cooling age, using Rb/Sr on biotite and feldspars, U-Pb on zircon and apatite), consists of three main magma pulses related to as many different facies (Sant'Andrea, San Francesco and San Piero facies in Farina et al., 2010) that produced the present composite plutonic body (Conticelli et al., 2001a; Dini et al., 2002; 2007; Gagnevin et al., 2004; 2008; Westerman et al., 2004; Rocchi et al., 2010). The dike swarm of the monzodioritic to granodioritic, at times mafic Orano Porphyry (dated 6.8 Ma, using Rb/Sr on biotite and feldspars, and $^{40}Ar/^{39}Ar$ methods on sanidine), pegmatites, aplites and leucogranites intruded the pre-Mt. Capanne laccolithic complex, the Mt. Capanne pluton, its contact aureole, and locally also the CU in central Elba (Dini et al., 2002; 2008; Rocchi et al., 2002; 2003).

Afterwards, the 6.2 to 5.9 Ma (obtained by K/Ar and Rb/Sr on biotite and $^{40}Ar/^{39}Ar$ methods on muscovite and biotite) Porto Azzurro Quartz-monzonite pluton was emplaced in the deepest levels of the tectonic stack (i.e. PU) in south-eastern Elba (Marinelli 1959; Saupé et al., 1982; Maineri et al., 2003; Musumeci et al., 2010). Mafic dikes are also present in the central-eastern part of the island (Fig. 1), i.e. the 5.8 Ma Mt. Castello dike ($^{40}Ar/^{39}Ar$ radiometric age on feldspar-rich groundmass, Conticelli et al., 2001b), the Case Carpini and the Mt. Capo Stella dikes (Pandeli et al., 2006; 2014). These dikes, as well as the Orano Porphyry, show petrographic and geochemical evidence of mixing between a calcalkaline mafic-intermediate magma similar to that of the Capraia Island and a crustal anatectic melt (Poli and Peccerillo, 2016).

THE MT. CAPANNE PLUTON AND ITS CONTACT METAMORPHIC AUREOLE

The 6.9 Ma Mt. Capanne Monzogranite represents an about 45 km^2 wide (10 km in diameter) plutonic body, that reached the shallower structural levels in the Elba tectonic stack (Bortolotti et al., 2001a; Westerman et al., 2004; Rocchi et al., 2010; Principi et al., 2015a; 2015b) intruding the Ligurian Nappes (i.e. PFU) (Figs. 1 and 2). The present wide outcrops of the Mt. Capanne pluton are also due to the important elisions of the Ligurian cover above the top (e.g. CEF) and along the flanks of the pluton and to the huge unroofing of the pluton (Bouillin et al., 1994; Dini et al., 2002; Farina et al., 2010). The asymmetrical shape of the pluton (characterized by a steeper western flank) was reconstructed through the distribution of magmatic foliations (see Table 1 in Boccaletti and Papini, 1989) and magnetic fabric (magnetic susceptivity in Bouillin et al., 1993; Cifelli et al., 2012). Bouillin et al. (1993) considered the Mt. Capanne intrusion as linked to an E-W-trending, sinistral main transcurrent fault locally characterized by "pull apart"-type extensional conditions. Instead, some Authors (Keller and Pialli 1990; Daniel and Jolivet 1995; Jolivet et al., 1998) suggested that the emplacement of the magmatic pluton was syn-tectonic and triggered by the development of low-angle faults linked to regional extensional tectonics. Other models, involving the contribution of regional tectonics vs. magmatic processes, were proposed by Bouillin (1983), Duranti et al. (1992), Pertusati et al. (1993), Bortolotti et al. (2001a) and Cifelli et al. (2012).

The contact aureole of the Mt. Capanne pluton crops out as a narrow aureole around the magmatic body, with the exception of the areas around Fetovaia to Cavoli and Punta Polveraia to Punta Cotoncello (to the S and NW of the pluton, respectively; Figs. 1 and 2) where it is not exposed. In the literature, the pressure values of ≤ 2 kbar reached by the PFU hornfels were established on the basis of chemical and petrographic data of the Mt. Capanne pluton, as well as on the geological data in agreement with the relatively shallow depth of the intrusion (4 to 6 km in Westerman et al., 2004; Rocchi et al., 2010; Rossetti et al., 2007). The temperature conditions in the host rocks during pluton emplacement were generally considered about 600°C (e.g., 575-625°C in Rossetti et al., 2007).

RESULTS

Lithostratigraphic data

The Authors (P.E., F.M.E., R.G.) performed the geological surveys of the host rocks of the Mt. Capanne pluton in the framework of the National Geological Map of Italy at 50.000 scale - Sheets 316, 317, 328, 329 “Isola d’Elba” of ISPRA (Geological Survey of Italy) (see geological map and explanatory notes in Principi et al., 2015a; 2015b; 2015c). Besides, Bortolotti et al. (2015) published an enlargement at the scale 1:25,000, with bilingual (Italian and English) legend and explanatory notes.

Seven lithological associations can be defined in PFU (Fig. 2b; the mineralogic abbreviations used in the text and in Tables 1 to 6 are from Whitney and Evans, 2010; locations of the outcrops in Fig. 2):

1- Serpentinites. These dark green to black, mostly massive rocks are well represented (Mt Perone-Bagno, Colle Palombaia-San Piero-Sant’Ilario and Punta Polveraia to Punta Fetovaia) and consist of serpentinites with steatite and magnesite veins generally transformed into Amp-rich hornfels (Plate 1a). Locally (e.g., Pomonte, Mt. Perone) the serpentinites are cut by metabasaltic dikes. The maximum apparent thickness is 100 m.

2- Metagabbros. They widely crop out between Mt. Perone and Bagno and in the Fetovaia Peninsula and are constituted by medium-, rarely coarse-grained, often massive meta-Mg gabbros, that locally includes dikes and bodies of dark green-black, Fe- and Ti-rich gabbros (Fetovaia Promontory and Pomonte). Mylonitic, flaser-type gabbros are common in the Fetovaia to Chiessi outcrops and their foliations are cut by meta-basaltic dikes that appear unfoliated at the mesoscale (e.g., south of Pomonte, see Plate 1b) and suggests a pre-Mt. Capanne origin for the flasering of such rocks. The maximum thickness is about 70 m.

3- Metaophiolitic breccia. It is locally (e.g, Fetovaia Promontory) present as a ≤2m-thick cover of the meta-gabbro and made up of gabbro and minor serpentinite clasts in a serpentinitic-chloritic matrix. Foliated grey-greenish to red ophicalcites are also present.

4- Metabasalts. Except for the San Piero-Sant’Ilario area, they are present in most of the outcrops of the metamorphic aureole and consist of locally foliated, massive or pillow-type (Plate 1c) metabasalts, dark green to brown-reddish in color. The maximum apparent thickness is 200 m.

5- Metacherts. They are common in most of the PFU outcrops (e.g. along the panoramic road between Pomonte and Fetovaia, Spartaia) and are represented by a well-bedded successions of thin (max 30 cm-thick) quartzitic strata of varicoloured (green, black/violet to whitish) meta-radiolarites with millimetric interbeds of siliceous meta-shales (Plate 1d). Their thickness locally exceeds 25 m.

6- Metalimestones Also this lithotype is common in many sectors of the aureole (e.g. along the panoramic road between Sedia di Napoleone to Punta Nera, south of Pomonte, east of Cavoli and at Spartaia) and consists of a well-bedded succession of foliated, decimetric up to 2.5m-thick whitish, greenish and grey, at times saccaroidal marbles with local calcschists intercalations. They also include microquartzitic lenses and bands (after cherts) that are generally folded at the outcrop scale (Plate 1e and f). At places (e.g. north of Punta Nera), thin Bt-rich metapelitic interbeds occur as well as an evident thermometamorphic blastesis of brown-reddish Grt and millimetric (max 1 cm) spherical/ellipsoidal Wo aggregates, generally characterized by either radiating- or rosette-type texture. The maximum thickness is 30 m.

7- Metashales and metalimestones. This association is present in the western outcrops of the aureole and also in the Marciana, Maciarello, Procchio and San Piero areas. It mainly consists of Bt-rich, dark grey, grey to grey-reddish metapelites, often characterized by a platy to scaly fabric, with intercalations of grey-greenish, more or less siliceous meta-limestones whose thickness is generally decimetric (Plate 1g). Wide metasomatic substitutions of the metacarbonate beds with calcsilicates (e.g. Grt and Wo) are locally recognizable (e.g. Punta della Fornace in Plate 1g). In the Marciana-Maciarello and locally in the Spartaia-Procchio areas, at least part of this lithological association consists only of metapelites and metasiltstones with rare metasandstone beds. The maximum apparent thickness of the formation (the stratigraphic top is not exposed) is about 80 m. This “complete”-type succession represents most of the outcrops of the metamorphic aureole (e.g. Pomonte-Fetovaia, Punta Nera-Punta Polveraia, Procchio-Spartaia and Marciana-Maciarello areas), but at places, it tectonically lies on “reduced”- type ones that show intrusive contacts with the underlying pluton. These latter are made up of: a) metashales and metalimestones including some meta-basalt bodies in the western side of Mt. Capanne, b) serpentinites with local basaltic dikes and metagabbros in the Mt. Perone-Bagno areas.

The PFU successions are intruded by the pre-Mt. Capanne dikes and laccolitic complex (8.5-7.4 Ma) that often appear foliated as the host rocks (Plate 1h) and both are cut by the undeformed granitoid intrusion. Typical examples are exposed in the western outcrops (Punta Nera-Punta Polveraia), at Spartaia-Procchio and at the Cavoli-Colle Palombaia beach and by the 6.8 Orano Porphyry dyke, aplites and leucogranites (e.g. Sant’Ilario Leucogranite). The Orano Porphyry dyke and the Sant’Ilario Leucogranite finally cut through the intrusive contacts of PFU with the granitoid (see Fig. 1).

Petrographic-mineralogic data

The petrographic analyses were performed on approximately 150 samples of hornfels collected in the different outcrops of the PFU (locations in Fig. 2). Some X-ray diffraction (XRD) mineralogic analyses were also performed to refine the microscopic observations. The compositional details for the rocks of each outcrop are shown in Tables 1-6. In the following paragraphs mineral abbreviations are from Whitney and Evans (2010). The An% content of the plagioclases was defined through petrographic methods (e.g. Michel-Levy method, Carlsbad-Albite method) and microprobe analyses (see following paragraph) and are reported in the Tables 1-6. The petrographic and mineralogic data for each formation of the PFU are summarized below (mineral abbreviation from Whitney and Evans, 2010):

1- Serpentinites (Table 1) show variable microscopic texture (nematoblastic, diablastic, lepidoblastic, fibroblastic and cellular) and mostly consist of Srp and Amp; the presence of Tlc is locally documented (Plate 2a). Where the foliation is more pervasive, iso-oriented porphyroclasts (usually Amp after Cpx) are locally present and characterized by asymmetric pressure shadows and micro-boudinage. Zonal crenulations affects both the main foliation and the Amp porphyroblasts. Anhedral oxides and hydroxides (mostly Fe minerals, e.g. Mag) locally lie parallel to the main foliation. In a few places (e.g. Punta Nera), the fine- to medium-grained blastesis of Ol after Srp (locally replacing relic cellular textures in the Ser + Amp fabric) is recognizable (Plate 2b). Later alterations assemblages made up of Cal and Chl are also present.

2- Metagabbros (Table 2) are characterized by granoblastic to porphyroblastic textures at the meso- and microscale (Plates1b and 2c). The porphyroblasts are made of Pl (with albite-carlsbad to polysyntetic twins) and Amp (Hbl and Tr-Act after Cpx) in a Pl + Amp groundmass. The contacts between host gabbros and the basaltic dikes are sometimes cut by metamorphic foliations at the microscale (Plate 2c). The primary accessory minerals are Py and Mag, whereas Spn is related to the metamorphism.

3- Metabasalts (Table 3) show a fine-grained nematoblastic to diablastic texture with Pl and Amp (Plate 2d); rare

Table 1 - Petrographic-mineralogical features of serpentinites.

CONTACT METAMORPHISM GRADE	TEXTURES	MINERALOGIC ASSOCIATIONS	VEINS	OUTCROPS (locations in Fig. 2)
LOW GRADE	Nematoblastic to diablastic to cellular	Srp (Ctl, after Ol) +Tr+ +Act±Ath+Tlc+Chl(Clc)	Qz±Chl±Ms/Ser; Mgs+Chl	3,6,7, 10, 11
Transition to MIDDLE GRADE	Nematoblastic, fibroblastic, diablastic to cellular	Srp(Ctl±Atg)+Tr+Ath+Tlc±Ol(±Hbl)	Grt+Ves+Ep±Chl±Py	1, 3, 6 (close to the contact with the pluton), 12
MIDDLE GRADE	Nematoblastic to cellular (relics)	Srp (generally Atg)+Ol(Fo86-88%)+Tr±Act+Tlc+ Ath	Chl+Py; Qz+Adl±Py	1,10, 11
Transition to HIGH GRADE	Nematoblastic/ diablastic to granoblastic	Ol(Fo=about 90mole%)+Tr±Hbl±Tlc		1, 4a, 5, 10a

Mineralogic abbreviations are from Whitney and Evans, 2010 as in the followings. In addition, An% range obtained in Pl: Ab= An_{8-10},Pl_{O1} (Na-rich oligoclase)= An_{11-18}, Pl_{O2}(Na-poor oligoclase)= An_{23-28}, Pl_A (andesine)= An_{34-48}, Pl_{LB} (labradorite-bytownite)=An_{65-82}, An=An_{90-94}.

Table 2 - Petrographic-mineralogical features of metagabbros.

CONTACT METAMORPHISM GRADE	TEXTURES	MINERALOGIC ASSOCIATIONS	VEINS	OUTCROPS (locations in Fig. 2)
LOW GRADE	Granoblastic, nematoblastic to flaser, locally porphyroblastic	Ab/Pl_{O1}+Tr-Act+Chl+Ep porphyroclasts of Amp+Ep (after pyroxene, sometimes relict at the core)		4
Transition to MIDDLE GRADE	Granoblastic to nematoblastic, locally porphyroblastic	Tr-Act + Pl_{O1}/Pl_{O2} + Grt±Hbl	Ep±Amp; Ep	3, 10
MIDDLE GRADE	Middle-grained granoblastic	Pl_{O2}/Pl_A+Tr-Act+Hbl(rare Qz in the groundmass)±Bt	Qz±Chl, Chl (Clc), Chl+Cal with Chl+Spn+Adl salband	4 (close to the pluton), 5, 10
Transition to HIGH GRADE	Middle- to coarse-grained granoblastic	Pl_A+Grt+Hbl±Bt±Di		1

Table 3 - Petrographic-mineralogical features of metabasalts.

CONTACT METAMORPHISM GRADE	TEXTURES	MINERALOGIC ASSOCIATIONS	VEINS	OUTCROPS (locations in Fig. 2)
LOW GRADE	Nematoblastic to sub-ophitic	Ab/Pl_{O1}+Chl± Tr-Act	Py	10
Transition to MIDDLE GRADE	Nematoblastic to sub-ophitic	- Pl_{O1}/Pl_{O2}+Tr-Act (+Phl, Chl) -Pl_{O2}+Tr-Act ±(Hbl)±amphibolized Di	Py	1,3 1,3
MIDDLE GRADE	Nematoblastic/diablastic	Pl_A+Hbl±Di±Grt(Adr) ±Ep	Qz+Amp	1, 4a, 5, 10, 10a
Transition to HIGH GRADE	Granonematoblatic to heteroblastic, locally porphyroblastic	Pl_A/Pl_{LB} +Hbl+Di+Qz(±Bt)±Ms Local intrafoliar lens with neoblastic Di+ Pl_{LB} ±Qz	Qz+Py+Spn	2,4a,5
HIGH GRADE	Granonematoblastic	Pl_{LB}+Di+Grt(Adr)±Bt		2, 10a

relics of ophitic texture were locally observed. Lens shaped porphyroclasts of Cpx and Pl (locally sericitized) in an overall Amp groundmass are recognizable in some samples. Small syn-kinematic polycrystalline augens of Cpx (Di) + Ms or lenticular bands of neoblastic Cpx and Pl locally occur within the main schistosity that is deformed by crenulation cleavages. Some big Cpx porphyroblasts contain deformed inclusion trails of opaque minerals. Syn-metamorphic accessory minerals are Spn, Py, Ep, Fe oxides and hydroxydes. Later Cal, Chl and Qz alterations and veins are common.

4- Metacherts (Table 4) are characterized by a fine to medium- grained granoblastic to granolepidoblastic texture that includes local porphyroblasts and syn-kinematic ribbons of mono and polycrystalline Qz (Plate 2e). Lenticular aggregates and millimetric levels of Ms ± Bt are sometimes present in the quartzitic mass. Static anhedral to sub-idiomorphic And (sometimes including Qz), Grt (generally Alm-rich, locally with Chl alterations) ± Crd are locally associated to these micaceous levels. Where the foliation is more pervasive, the Qz and And porphyroclasts show rotations and Qz-mica pressure shadows (i.e. mantled type σ and δ porphyroblasts, Plate 2f). Single or aggregated big mica (typically Bt) porphyroclasts often form typical mica fishes inside the main foliation. Rarely, small albite polysynthetic twinned Pl can also occur. At places (e.g. north of Punta Nera), Bt and Ms mica-fishes and porphyroclasts are present inside the main foliation and in some cases include small blasts of sub-idiomorphic Crd. Concentrations of fine-grained, anhedral Fe oxides and hydroxides of iron are frequently present as discontinuous bands in the quartzitic mass parallel to the main schistosity. The presence of Hc was determined in the meta-cherts at the Colle Palombaia beach (Plate 2g) close to a small apophysis of the underlying granitoid. Primary accessory minerals are Zrn and Py, whereas Ap, Rt, Fe oxides and hydroxides, Mnz are related to the metamorphism.

5- Metalimestones (Table 5). Their often foliated marbles and calcschists are characterized by a granoblastic to polygonal mosaic-like Cal framework (with plane to concave -convex, rarely sutured, crystalline junctions) and locally by mylonitic texture. Sometimes the polygonal calcitic texture is heteroblastic with centimetric/millimetric bands of different blast sizes (from 50 mμ to about 2mm). Fine- to coarse-sized xenoblasts of Cpx (mostly Di) and Qz are frequently spread in the Cal mass. Deformations of the twins in the Cal blasts are particularly evident in the coarse-grained metacarbonate rocks; in particular type II and, rarely, type III twinnings (according to Burkhard, 1993 and Ferril et al., 2004) were observed. Moreover, in the more recrystallized samples we found: a) lenticular and/or ribbon-shaped levels of medium- to fine-grained Wo, of Wo + Cpx (± And) (Plate2h), of Grt (Grs) + Di + anortitic Pl + Wo, Wo + Ves and of Cpx + Grt(Grs) ± meionitic Scp (likely after Pl) ± Ves that lie parallel to the main schistosity and are deformed by a successive folding (Plate 2i); b) Wo, Cpx (Di to Aug) and rarely Qz locally formed single porphyroblasts or are arranged in clusters often showing rotations respect to the main foliation (Plate 2j); c) Grt, Ves and Scp porphyroblasts host Di and Wo inclusions; d) Locally, Wo + Cpx, Ves ± Wo (Plate 2l), Cpx and/or Grt metasomatically replace most parts of the carbonatic rocks with the formation of exoskarns (e.g. the skarns at Procchio-Punta dell'Agnone).

At places (e.g. north of Punta Nera, south of Punta Polveraia beach), Wo forms either typical millimetric fans or sphaeric to ellisoidal radiating- type clusters that are flattened parallel to- and enveloped within the main foliation; however post-kinematic Wo radiating sphaerules, sometimes with Di at the core (Plate 2k) and at the rims (as Cpx micro-granoblasts), are also common. A later chloritization of the femic minerals can be locally recognized. Accessory metamorphic minerals are Spn, Fe oxides/hydroxides, Py, Ep, Ap.

The original shaly-marly intercalations are transformed either into Bt- or, rarely, into Amp-rich layers and frequently show brittle boudinage with respect to the ductile behaviour of the marble (see also Fig. 7 in Bouillin, 1983; Daniel and Jolivet, 1995).

Discontinuos, millimetre to centimetre-thick veins of Ves + Grt ± Wo with a Wo salband (vein margin) are well recognizable in the Spartaia - Punta dell'Agnone outcrops (site 9 in Fig. 2, see also Rossetti et al., 2007). These veins, that lie parallel and subordinately perpendicular to the main schistosity, are common in the metapelitic-calcschists layers whereas are rare in the marble beds; elsewhere Cpx + Scp + anortitic Pl veins were also recognized. These veins are cut by later ones containing lower temperature assemblages of hydrothermal mineral associations (e.g. Qz ± Cal, Cal + Adl). In several areas (e.g. Marmi, Procchio - Spartaia and Cavoli), where the contact between the carbonatic hornfels and the pluton is exposed, it is often underlined by a mas-

Table 4 - Petrographic-mineralogical features of metacherts.

CONTACT METAMORPHISM GRADE	TEXTURES	MINERALOGIC ASSOCIATIONS	VEINS	OUTCROPS (locations in Fig. 2)
LOW GRADE	Granoblastic	Qz±Ms/Ser±Chl±Bt		3.4
Transition to MIDDLE GRADE	Granoblastic to granolepidoblastic	- Qz+Bt+Ms±Grt(Alm)±Crd(±And)	Qz+Ser/Ms (syn-kynematic)	3,6,10, 11
		- Qz+Bt±Ms±Crd		3,9,12
		- Qz+Di+Bt+Ms/Ser		1,12
		- Qz±int.Pl+Hbl+Ep+Di ±Grt		1
MIDDLE GRADE	Granonblastic to granolepidoblastic	- Qz+Bt+Di (Di) + Ep + Hbl + Ms ± Tr-Act±Crd±And		3
Transition to HIGH GRADE	Granonoblastic to granolepidoblastic	- Qz+Bt±int.Pl		5 (panoramic road), 9
		- Qz+Bt+Di		
		- Qz+Bt+Di±Cal	Cal+Qz; Chl±Cal with Qz salband; Chl±Qz	
	Lepidoblastic to granolepidoblastic (metapelite intercalation)	Bt+Qz± Pl_A+And±Grt(Alm)±Ms (+Hc)		5
HIGH GRADE	Granonoblastic to granolepidoblastic	- And±Di±Grt(Alm)±PlA/PlLB±Hc±Mnz+Ms± Qz		5 (Colle Palombaia beach)
		- Qz+Scp+Kfs±Crd		9

Table 5 - Petrographic-mineralogical features of metalimestones.

CONTACT METAMORPHISM GRADE	TEXTURES	MINERALOGIC ASSOCIATIONS	VEINS	OUTCROPS (locations in Fig. 2)
LOW GRADE	Very fine-grained granoblastic	- Cal±Qz - Cal±Qz±Ab/Pl$_{O1}$±Ep		4 3
Transition to MIDDLE GRADE	Granoblastic	- Cal±Qz± Pl$_{O1}$/Pl$_{O2}$±Di±Bt; - Cal+Qz+Di+Bt±Ep±Chl		3
MIDDLE GRADE	Granoblastic	- Cal+Di± Pl$_{O2}$/Pl$_{A}$±Bt - Cal+Tr+ Pl$_{A}$+Di±Qz - Cal+Di+ Pl$_{A}$±Qz± Grt (±Wo)	Qz+Cal+Wo Grt+Ves±Di (syn-tectonic in the amphibolitic levels)	5 8 3
	lepidoblastic/nematoblastic (marly-pelitic intercalations)	Bt±Ms or Amp		
Transition to HIGH GRADE	Granoblastic, xeno- to homeoblastic	- Cal+Di+Hd+ Pl$_{A}$ /Pl$_{LB}$±Bt - Cal+Di±Wo±Qz - Cal+Di+Ms+Bt±Ms±Wo±Qz	Cal, Fe Ox/hydroxides+Chl, Bt	1,5,8,9
	Lepidoblastic/nematoblastic (marly-pelitic intercalations)	- Bt±Cal±Spn±Py - Bt+Py +Hem±Wo	Cal+Adl+Chl+Tr-Act	07/01/18
HIGH GRADE	Granoblastic to polygonal, xeno- to homeoblastic, locally heteroblastic	- Cal+Di (+Hd)+Kfs+ Pl$_{LB}$+Bt - Cal+Di+Wo+Ep - Cal+Grs(Grs-Adr) + Di + Ves+ +Scp+Wo+Kfs+ Pl$_{A}$ /Pl$_{LB}$ ±Ms - Cal+Di+Wo±Qz±And±Grt±Scp - Cal(±FeCal)+Di+Wo+Scp; - Wo+Di	Qz+Cal+Wo; Cal; Di+Scp±Qz; Cal+Qz+Ep±Chl; Cal+Qz Grs+Wo ±Ves Qz Cal+Ad	5,8,9,11, 3 (only at the contact with the late acidic dykes) 1, 9
	Lepidoblastic (marly-pelitic intercalations)	- Bt±Qz ±Cal±Di±Crd - Bt+Di+ Pl$_{LB}$+Crd+Kfs - Bt+Crd+ Pl$_{LB}$/An +Kfs±Qz	Di+Scp; Ad+Py	5,9

sive, brown to greenish horizon (see Fig. 2 in Rossetti et al., 2007), decametric to metric in thickness, and characterized by a granoblastic texture made up of calc-silicates (intermediate Pl + Qz + Bt + Kfs, Cpx + intermediate Pl + Kfs ± Scp, or Ves + Grs + Cpx + Wo + intermediate-calcic Pl ± Kfs or Cpx + intermediate Pl + Scp).

6- Metashales and metalimestones (Table 6). Their main shaly and siltitic protoliths are recrystalized into with lepidoblastic to granolepidoblastic, Bt-rich, more or less quartzose metapelites. The metacarbonate beds are transformed into granoblastic marbles that locally include Wo (even millimetric to centimetric sphaerical radiating clusters in Plate 1g), Cpx and Grt (generally Grs) locally present as aggregates in brownish-reddish levels, centimetric in thickness) that appear as syn-kinematic, but sometimes overprint the main foliation. In some outcrops (e.g. Punta della Fornace), most of the marble beds are transformed in exoskarns. Alternating bands of Bt + Cpx ± Wo ± Qz and Cpx + Grt + Wo ± Scp are locally recognizable in the more recrystallized marbles (e.g. Spartaia area). Later Chl alterations are locally common. The rare metasandstone beds (more frequent in the area10) are transformed in more or less micaceous quartzites. Primary accessory minerals are Py and Zrn whereas Spn, Ep, Tur, Fe oxides/hydroxides can be referred to metamorphic processes.

7- Metaporphyritic dikes are characterized by porphyroclastic textures with feldspatic porphyroclasts sometimes arranged as clusters. They are Ab-Carlsbad to Ab polysynthetic twinned Pl (sometimes with anhedral Qz rims) and Kfs (with locally preserved mirmekitic textures and Qz and Bt inclusions) (Plate2 m). Quartz porphyroclasts (sometimes as clusters) are locally frequent and preserve their original structures, e.g. rounded shape and local embajements (Plate 2n). The Pl and Kfs porphyroclasts and in the groundmass are more or less altered into Cal and Ser. Tur coronas of the feldspar porphyroclasts can be also recognized. The foliated groundmass is granoblastic to granolepidoblastic and consists of Qz, Pl, Kfs and Bt. Millimetric (up to some centimeter in size) porphyroclasts of Tur are common in the foliated Portoferraio Porphyry-like bodies and form bands and "trains" textures within the foliation, locally with domino-like textures (Plate 2m). Accessory minerals are mostly magmatic: Tur, Zrn, Ap, Mnz, Aln and Py (Portoferraio-like metaporphyries) and Zrn, Ap, Mnz, rare Tur (San Martino-like metaporphyries).

Mineral chemistry data

Selected chemical analyses of most minerals in the metalimestones, metacherts, serpentinites amphibolites and metagabbros/basalts are reported in Table 7. Furthermore, EDS spectra and/or WDS analyses allowed to identify other minerals whose analyses are not reported here. The detected minerals were Aln, Cal, Bt, Ms, Zrn, Sp and Rt in metalimestones; Chl, Qz, Tur, Bt, Ms, And Kfs, Zrn, Ap in metacherts; Chl, Ap and Ilm in metaserpentinites; Ap in meta-gabbros.

Clinopyroxenes in metalimestones have variable MgO and FeO contents, so that they are classified as both Di and Hd, according to the official nomenclature (Morimoto, 1988). Locally Wo also occurs and contains small amounts of FeO (0.3-0.5 wt%) MnO (0.2 -0.3 wt%) and MgO (0.1-0.2 wt%).

Garnets, detected in both metalimestones and metacherts,

Table 6 - Petrographic-mineralogical features of metashale and metalimestones.

CONTACT METAMORPHISM GRADE	TEXTURES	MINERALOGIC ASSOCIATIONS	VEINS	OUTCROPS (locations in Fig. 2)
	Domainal schistosity to Lepidoblastic (metapelite)	- Bt+Ms/Ser±Qz±Cal±clay minerals	Ep, Chl, Qz+Cal±Ep in Chl salband	4
		- Bt+Chl+Cal+Ser/Ms		3
Very LOW GRADE/LOW GRADE	Weakly recrystallized (fine-grained granoblastic) (marble)	Cal		3,4
	Granoblastic-xenoblastic (metasandstone level)	Qz+Bt+Ms±Chl	Qz; Qz+Ms+Chl; Qz+Tur+Ms+Py	3
Transition to MIDDLE GRADE	Lepidoblastic (metapelite)	Bt±Qz±Ms	Qz±FeOx	2,6, 11,12
	Granoblastic (metasandstone level)	Qz±Bt±Pl_{O1}/Pl_{O2}±Tr± Grt		1
	Lepidoblastic (metapelite)	- Bt+Ms±Tr-Act ± And + Qz ± Crd + Pl_{O2}/Pl_A+Di+Hd	Di+ Pl_A/Pl_{LB}+Bt; Ad+Ep	3
MIDDLE GRADE		- Bt+Grt+Di±Cal±Qz	Di+ PlA+Bt; Ad+Ep	6, 10, 11,12
	Granoblastic to polygonal (marble)	Cal+Di+Grt± PlO2/PlA±Qz		6, 3
	Polygonal heteroblastic (marble)	- Cal+Wo+Di (+Hd)±Qz±Bt±Ms		1
		- Cal+Di+Hd+Wo+Grt+Ep	Cal	2
Transition to HIGH GRADE		- Cal+Di+Grt± Pl_A/Pl_{LB}		3
	Lepidoblastic (metapelite)	Bt±Qz±Ms		2,3
	Granoblastic to polygonal floor-type (marble)	- Cal+Di+Wo+Scp+Grt+Bt (±Ms)	Ep	1, 2, 2a,4a,9
		- Di±Wo±Cal±Ep	Ep±Wo±Cal±Di±Spn	1,2
		- Grt+Di+Wo±Ves		1,2
		- Cal+Wo+Di+Grt+Ep		2
		-Wo+Di	Qz; Ca+Wol	2, 11
HIGH GRADE	Granolepidoblastic to lepidoblastic (metapelite)	- Bt+Di (+ Hd)+Wo+Grt (±Ms±Qz)	Ep	2
		- Bt+And+ Pl_{LB} /An+Ms+Kfs+Di±Crd		1
		- Bt+Di+Hd+Grt+Wo±Ves±And±Ep	Di+Spn	2
		- Bt+Di+Grt+Wo+Qz±And±Ves±Ep		2,9
		- Bt+Di+ Pl_{LB} /An+Crd+Kfs		4a
		- Bt+Crd+ Pl_{LB} /An		4a
		- Bt+Di+Pl_{LB} /An +Ep		4a

have a quite different composition depending upon the nature of the protolith. In fact, crystals from the former group pertain to the ugrandite (Grs- 78-85 mol%, Adr- 10-20 mol%) series, whereas garnets in metacherts belong to the pyralspite series (Alm- 56-75 mol%, Sps- 22-38 mol%). Sometimes a weak zoning is detectable in crystals with rims showing greater amounts of Adr in metalimestones or Alm in metacherts with respect to the cores.

Vesuvianites in the metalimestones have TiO_2 contents up to 3.4 wt%. Similar values have been found in Ves occurring in the calc-silicate hornfels of the Procchio area (Rossetti et al., 2007).

Spinels in metacherts have considerable ZnO contents (10-16 wt%) and they can be considered as solid solutions of mainly Hc ($FeAl_2O_4$, 54-69 mol%) and Ghn ($ZnAl_2O_4$, 24-39 mol%). On the other hand, spinels in serpentinites have considerable Cr contents and the Chr ($FeCr_2O_4$) component is about 25 mol%.

Feldspars in the metalimestones, Pl (oligoclase, since Ab is in the range 73-76 mol%) coexists with almost pure An (95 mol%). On the contrary, more albitic oligoclase (Ab = 82-89 mol%) coexists with Kfs (containing up to 16 mol% of Ab) in the metacherts. Pl with similar composition was found in the metabasalts.

Epidote found in the metalimestones has a formula approximated to $Ca_2(Fe,Al)_3(SiO4)_3(OH)$. Epidotes belongs to the clinozoisite subgroup and they can be classified as clinozoisites (Armbruster et al., 2006). Their FeO contents is about 6.7 wt%.

Amphiboles in the metabasalts and in the serpentinites belong to the Ca group. According to the nomenclature of amphiboles (Leake, 1978) they can be classified as actinolitic Hbl in metabasalts and Tr and Act in serpentinites.

Neoblastic Olivines are present in the serpentinites and have Fo contents about 90 mol%.

Tables 7 - Electron microprobe analyses (data in wt%) of clinopyroxenes (Cpx), wollastonites (Wo), garnets (Grt), vesuvianites (Ves), spinels (Spl), feldspars (Fsp), epidotes (Ep), amphiboles (Am) and olivines (Ol) in metalimestones (Mlim.), metacherts (Mcher.), serpentinites (Serp.) and metagabbros/basalts (Mbas.).

Mineral	Cpx	Cpx	Cpx	Cpx	Cpx	Wo	Wo	Wo
Rock	Mlim.	Mlim.	Mlim.	Mlim.	Mlim.	Mlim.	Mlim.	Mlim.
Sample	PN6	cavo	pn5	POL-2	POL-2	pn5	pn4	pn5
SiO_2	51.35	51.26	51.13	49.68	48.52	51.13	51.57	51.29
TiO_2	0.15	0.11	0.03	0.11	bdl	0.02	bdl	bdl
Al_2O_3	2.27	0.33	0.31	0.12	0.26	0.02	0.06	0.01
Cr_2O_3	0.15	bdl	0.02	0.08	bdl	bdl	bdl	0.02
FeO	10.24	12.85	15.92	20.94	27.15	0.32	0.42	0.50
MnO	0.34	0.60	0.23	1.54	0.48	0.27	0.32	0.33
MgO	10.66	9.10	8.04	3.90	0.73	0.26	0.18	0.15
CaO	25.17	23.86	23.98	22.76	22.28	46.84	46.73	46.57
Na_2O	bdl	0.15	0.08	0.03	0.11	0.04	bdl	bdl
K_2O	bdl	0.06	bdl	0.11	bdl	bdl	0.11	0.11
ZnO								
Sum	100.33	98.32	99.74	99.28	99.53	98.90	99.38	98.97
Cations per 6 O.								
Si	1.938	2.002	1.988	2.006	1.998	2.000	2.006	2.005
^{IV}Al	0.062	0.000	0.012	0.000	0.002	0.000	0.000	0.000
Fe^{3+}	0.000	0.000	0.000	0.000	0.000	0.000	0.000	0.000
sum	2.000	2.002	2.000	2.006	2.000	2.000	2.000	2.000
^{VI}Al	0.039	0.015	0.002	0.006	0.011	0.001	0.003	0.000
Fe^{3+}	0.010	0.000	0.014	0.000	0.000	0.000	0.000	0.000
Ti	0.004	0.003	0.001	0.003	0.000	0.000	0.000	0.000
Mg	0.600	0.530	0.466	0.235	0.045	0.015	0.010	0.009
Cr	0.005	0.000	0.001	0.003	0.000	0.000	0.000	0.000
Fe^{2+}	0.313	0.451	0.516	0.753	0.944	0.011	0.014	0.016
Na	0.000	0.011	0.006	0.002	0.009	0.003	0.000	0.000
Mn	0.011	0.020	0.007	0.053	0.017	0.009	0.010	0.011
Ca	1.018	0.998	0.999	0.985	0.983	1.962	1.947	1.950
sum	2.000	2.029	2.012	2.039	2.009	2.001	1.984	1.987
End members (mol%):								
wollastonite	52.14	50.71	50.18	49.73	49.64			
enstatite	30.73	26.94	23.42	11.87	2.26			
ferrosilite	17.13	22.35	26.40	38.40	48.10			
classification	diopside	diopside	hedenbergite	hedenbergite	hedenbergite			

Mineral	Grt	Grt	Grt	Grt	Grt	Grt	Grt	Grt	Grt
Rock	Mcher.	Mcher.	Mcher.	Mcher.	Mcher.	Mlim.	Mlim.	Mlim.	Mlim.
Sample	R4	R4	R8	R1-R3	R1-R3	PN6	pn4	pn5	POL-2
SiO_2	35.90	36.20	35.86	35.49	35.76	38.03	38.64	38.98	38.41
TiO_2	0.09	0.04	0.17	0.00	0.24	0.67	0.90	0.37	0.33
Al_2O_3	20.67	21.05	20.55	20.09	20.50	18.49	18.77	20.08	18.50
Cr_2O_3	0.05	bdl	0.07	0.08	0.04	0.08	0.23	bdl	bdl
FeO	29.99	29.12	24.92	28.24	28.26	5.76	5.99	4.97	6.34
MnO	11.36	11.53	16.03	14.88	13.45	0.63	0.24	0.31	0.27
MgO	1.18	0.94	0.26	0.33	0.23	0.03	0.19	0.23	0.24
CaO	0.27	1.02	1.59	0.91	0.70	35.94	34.24	34.66	35.03
Na_2O	bdl	bdl	bdl	0.05	0.09	bdl	0.10	bdl	bdl
K_2O	bdl	bdl	bdl	0.09	0.04	bdl	bdl	0.01	0.11
ZnO	bdl					0.13			
Sum	99.51	99.90	99.43	100.15	99.31	99.76	99.28	99.61	99.23
Cations per 24 O.									
Si	5.913	5.930	5.928	5.845	5.929	5.800	5.946	5.950	5.907
^{IV}Al	0.087	0.070	0.072	0.155	0.071	0.200	0.054	0.050	0.093
sum	6.000	6.000	6.000	6.000	6.000	6.000	6.000	6.000	6.000
^{VI}Al	3.925	3.993	3.930	3.744	3.934	3.123	3.349	3.561	3.261
Fe^{3+}	0.135	0.067	0.092	0.436	0.110	1.010	0.497	0.408	0.779
Ti	0.011	0.005	0.021	0.000	0.029	0.076	0.104	0.042	0.038
Mg	0.291	0.230	0.064	0.080	0.057	0.007	0.044	0.052	0.056
Cr	0.006	0.000	0.009	0.010	0.005	0.010	0.028	0.000	0.000
Fe^{2+}	3.999	3.925	3.357	3.457	3.812	0.000	0.274	0.228	0.037
Mn	1.586	1.600	2.246	2.077	1.890	0.081	0.031	0.040	0.035
Ca	0.048	0.179	0.281	0.161	0.125	5.872	5.644	5.668	5.772
sum	10.000	10.000	10.000	9.965	9.963	10.179	9.972	9.998	9.978
uvarovite	0.15	0.00	0.22	0.26	0.13	0.25	0.71	0.00	0.00
andradite	0.66	1.70	2.32	2.53	1.99	19.00	12.65	10.27	19.79
pyrope	4.92	3.87	1.08	1.38	0.97	0.13	0.75	0.87	0.95
spessartine	26.80	26.97	37.87	35.98	32.12	1.40	0.52	0.68	0.59
grossular	0.00	1.31	2.20	0.00	0.00	79.23	82.44	85.01	78.04
almandine	67.47	66.14	56.31	59.85	64.79	0.00	2.93	3.17	0.63

Mineral	Ves	Ves	Ves	Ves
Rock	Mlim.	Mlim.	Mlim.	Mlim.
Sample	cavo	cavo	POL-2	POL-2
SiO_2	36.32	35.43	35.93	34.95
TiO_2	0.38	1.49	3.26	3.37
Al_2O_3	17.20	16.09	15.02	14.77
Cr_2O_3	0.01	bdl	bdl	0.02
FeO	3.90	4.14	4.52	4.34
MnO	0.19	0.17	bdl	bdl
MgO	2.12	1.40	1.42	1.38
CaO	34.53	34.50	33.99	34.09
Na_2O	0.11	0.09	bdl	0.09
K_2O	0.09	0.07	0.04	bdl
ZnO				
Sum	94.85	93.37	94.19	93.01
Cations per 74 O.				
Si	18.232	18.160	18.249	18.032
Ti	0.143	0.574	1.243	1.306
Al	10.196	9.737	9.005	8.995
Fe^{2+}	1.638	1.776	1.923	1.876
Mn	0.080	0.075	0.000	0.000
Mg	1.584	1.068	1.077	1.059
Ca	18.566	18.940	18.494	18.839
Na	0.103	0.088	0.001	0.088
K	0.057	0.045	0.026	0.000
Cr	0.006	0.000	0.000	0.010
sum	50.604	50.463	50.019	50.204

Mineral	Spl	Spl	Spl
Rock	Mcher.	Mcher.	Serp.
Sample	R4	R4	PALO 4
SiO_2	bdl	0.07	bdl
TiO_2	0.04	0.08	0.55
Al_2O_3	54.52	54.46	28.45
Cr_2O_3	bdl	bdl	28.49
FeO	19.78	25.51	31.28
MnO	0.57	0.66	0.40
MgO	0.94	0.96	5.93
CaO	bdl	bdl	0.11
Na_2O	bdl	bdl	0.12
K_2O	bdl	bdl	bdl
ZnO	16.02	10.15	
Sum	91.88	91.89	95.31
Formula on the basis of 24 cations.			
Si	0.000	0.018	0.000
Ti	0.008	0.016	0.108
Al	16.306	16.189	8.762
Cr	0.000	0.000	5.888
Fe^{3+}	0.000	0.000	1.135
Fe^{2+}	4.202	5.385	5.708
Mn	0.123	0.141	0.089
Mg	0.357	0.362	2.311
Zn	3.003	1.890	
ulvospinel	0.10	0.19	1.35
spinel	4.65	4.65	15.82
magnesioferrite	0.00	0.00	2.05
magnesiochromite	0.00	0.00	10.63
hercynite	54.57	69.05	38.33
magnetite	0.00	0.00	4.96
chromite	0.00	0.00	25.76
galaxite	1.60	1.81	0.97
jacobsite	0.00	0.00	0.13
franklinite	0.00	0.00	
gahanite	39.07	24.30	

Fe^{2+} and Fe^{3+} calculated from charge balance, when reported. In particular, amphiboles were recalculated using Probe-Amph (Tindle and Webb, 1994) adjusting total cations (excluding Ca + Na + K) to 13.

Table 7 (*continued*)

Mineral	Fsp	Fsp	Fsp	Fsp	Fsp	Fsp	Fsp	Fsp	Fsp	Fsp	Fsp	Fsp
Rock	Mlim.	Mlim.	Mlim.	Mlim.	Mcher.	Mcher.	Mcher.	Mcher.	Mcher.	Mbas.	Mbas.	Mbas.
Sample	cavo	cavo	PN6	pn4	R8	R8	R8	R1-R3	R1-R3	R1	R1	R1
SiO_2	61.26	61.97	45.69	43.50	65.14	63.77	64.64	64.78	65.61	65.10	65.73	65.18
TiO_2	0.11	bdl	bdl	bdl	0.07	0.04	bdl	0.09	0.02	0.08	0.08	bdl
Al_2O_3	23.80	23.93	33.26	35.65	18.83	22.22	22.19	18.07	21.66	22.38	21.19	21.99
Cr_2O_3	0.03	bdl	0.06	bdl	0.04	0.05	0.05	0.03	bdl	0.01	bdl	0.01
FeO	0.17	0.05	0.61	0.17	0.03	0.10	bdl	bdl	0.04	0.01	0.08	0.38
MnO	0.04	0.05	0.17	bdl	0.12	0.03	bdl	0.03	0.01	0.04	0.02	bdl
MgO	0.01	0.07	0.01	0.04	0.01	bdl	0.02	bdl	0.03	bdl	bdl	0.04
CaO	5.57	5.10	19.07	18.71	0.09	3.26	3.19	0.09	2.24	3.09	2.82	3.10
Na_2O	8.69	8.90	0.58	0.48	1.16	9.75	8.88	1.77	10.24	9.50	9.80	9.68
K_2O	bdl	0.02	0.02	0.17	14.61	0.37	0.23	14.00	0.17	bdl	0.08	0.06
Sum	99.67	100.09	99.45	98.70	100.10	99.58	99.20	98.85	100.03	100.20	99.82	100.43
Cations per 8 O.												
Si	2.735	2.748	2.126	2.036	2.992	2.832	2.862	3.009	2.884	2.857	2.896	2.858
Al	1.252	1.251	1.824	1.970	1.020	1.163	1.158	0.989	1.122	1.157	1.100	1.136
Fe	0.007	0.002	0.026	0.007	0.001	0.004	0.000	0.000	0.002	0.001	0.003	0.015
sum	3.994	4.001	3.976	4.012	4.013	4.000	4.020	3.998	4.008	4.015	3.999	4.010
Ca	0.266	0.242	0.951	0.938	0.004	0.155	0.151	0.004	0.106	0.145	0.133	0.146
Na	0.752	0.765	0.052	0.044	0.104	0.839	0.763	0.159	0.873	0.808	0.837	0.823
K	0.000	0.001	0.001	0.010	0.856	0.021	0.013	0.829	0.010	0.000	0.005	0.004
sum	1.018	1.009	1.004	0.992	0.964	1.015	0.927	0.993	0.988	0.954	0.975	0.972
sum	5.012	5.009	4.980	5.004	4.977	5.015	4.947	4.991	4.995	4.969	4.974	4.982
End members (mol%):												
anorthite	26.16	24.00	94.67	94.58	0.44	15.28	16.34	0.45	10.69	15.25	13.65	14.97
albite	73.84	75.87	5.21	4.39	10.74	82.67	82.27	16.03	88.34	84.74	85.86	84.67
orthoclase	0.00	0.13	0.11	1.03	88.82	2.05	1.39	83.52	0.97	0.01	0.49	0.36
classification	oligocl	oligocl	*anorthite*	*anorthite*	K-feld	oligocl	oligocl	K-feld	oligocl	oligocl	oligocl	oligocl

Mineral	Ep
Rock	Mlim.
Sample	POL-2
SiO_2	37.99
TiO_2	0.20
Al_2O_3	27.42
Cr_2O_3	0.04
FeO	6.65
MnO	0.04
MgO	bdl
CaO	23.29
Na_2O	0.03
K_2O	0.02
Sum	95.67
Cations per 25 O.	
Si	6.006
Al	5.108
Fe^{3+}	0.892
Ti	0.024
Mn	0.005
Mg	0.000
Ca	3.946
K	0.004
sum	15.985

Mineral	Am	Am	Am	Am	Am	Am	Am	Am
Rock	Mbas.	Mbas.	Mbas.	Mbas.	Serp.	Serp.	Serp.	Serp.
Sample	R1	R1	R1	R1	PALO 4	PALO 4	PALO 4	POM 4
SiO_2	51.36	51.29	50.22	50.68	56.75	56.84	55.62	58.70
TiO_2	0.45	0.46	0.57	0.61	bdl	0.05	0.04	0.15
Al_2O_3	3.32	3.84	4.17	3.85	1.10	0.90	1.36	0.06
Cr_2O_3	bdl	bdl	0.07	bdl	bdl	0.09	0.06	0.02
FeO	15.48	15.49	15.65	15.67	4.45	4.11	6.11	1.39
MnO	0.43	0.47	0.33	0.28	0.13	0.23	0.21	0.09
MgO	13.97	13.97	13.32	13.57	22.67	22.21	19.58	24.02
CaO	10.53	10.29	10.48	10.46	12.07	12.03	12.14	12.62
Na_2O	0.90	0.95	1.38	1.07	0.18	0.08	0.22	0.01
K_2O	0.16	0.17	0.14	0.09	bdl	0.13	0.01	bdl
Sum	96.59	96.94	96.32	96.28	97.34	96.67	95.36	97.05
Cations per 23 O.								
Si	7.440	7.381	7.348	7.382	7.768	7.830	7.878	7.993
^{IV}Al	0.560	0.619	0.652	0.618	0.177	0.146	0.122	0.007
^{VI}Al	0.006	0.032	0.068	0.043	0.000	0.000	0.105	0.002
Ti	0.049	0.050	0.063	0.067	0.000	0.005	0.004	0.015
Cr	0.000	0.000	0.008	0.000	0.000	0.010	0.007	0.002
Fe^{3+}	0.905	1.019	0.747	0.857	0.509	0.473	0.254	0.158
Fe^{2+}	0.970	0.846	1.168	1.052	0.000	0.000	0.470	0.000
Mn	0.053	0.057	0.041	0.035	0.015	0.027	0.025	0.010
Mg	3.017	2.997	2.906	2.947	4.626	4.561	4.135	4.876
Ca	1.634	1.586	1.643	1.632	1.770	1.776	1.842	1.841
Na	0.253	0.265	0.392	0.302	0.048	0.021	0.060	0.003
K	0.030	0.031	0.026	0.017	0.000	0.023	0.002	0.000
sum	16.92	16.88	17.06	16.95	16.91	16.87	16.90	16.91
classification	ferrian-actinolitic hornblende	ferri-actinolitic hornblende	actinolitic hornblende	ferrian-actinolitic hornblende	tremolite	tremolite	actinolite	tremolite

Mineral	Ol	Ol	Ol
Rock	Serp.	Serp.	Serp.
Sample	POM 4	POM 4	POM 4
SiO_2	40.09	41.38	40.43
TiO_2	0.08	0.07	0.17
Al_2O_3	bdl	0.05	0.01
Cr_2O_3	0.06	0.04	0.02
FeO	9.32	9.51	9.58
MnO	0.21	0.13	0.18
MgO	49.76	49.22	48.34
CaO	0.08	0.17	0.13
Na_2O	bdl	bdl	bdl
K_2O	bdl	bdl	bdl
Sum	99.59	100.59	98.86
Cations per 4 O.			
Si	0.987	1.007	1.003
Fe	0.192	0.194	0.199
Mn	0.004	0.003	0.004
Mg	1.827	1.786	1.788
Ca	0.002	0.004	0.003
sum	2.026	1.987	1.994
forsterite	90.49	90.21	89.99
fayalite	9.51	9.79	10.01

Fe^{2+} and Fe^{3+} calculated from charge balance, when reported. In particular, amphiboles were recalculated using Probe-Amph (Tindle and Webb, 1994) adjusting total cations (excluding Ca + Na + K) to 13.

Structural data

The host rocks (PFU) of the Mt. Capanne pluton suffered both ductile (including the local development of mylonitic shear zones) and later brittle polyphase deformations. Given the variability of the lithologic association of the protoliths, the distribution of deformative features can be different within each lithotype association of the metamorphic aureole.

Ductile structures

Ductile structures are well recognizable in the metasedimentary formations and particularly in marbles and calcschists with the development of foliations and folds, as well as in a part of the dike complexes older than the Mt. Capanne pluton (i.e. the Portoferraio and San Martino Porphyry, see below).

Folds

Two ductile deformation events (D_1 and D_2) and a weak later folding (D_3) event are recognizable in the PFU:

D_1 is represented by continuous-type S_1 foliation (mm/sub-mm in size with Cal + Qz + Ms/Ser and opaque minerals) that is generally parallel to the S_0 bedding surfaces in most of the metasedimentary lithotypes (Fig. 3). D_1 folding structures associated to the S_1 foliation are rarely observed in the field (i.e. Fetovaia, Cavoli and Spartaia areas). They are generally recumbent, sometimes unrooted isoclinal folds, cm-dm in size, often with a sheath fold geometry (Passchier and Trouw. 1996). The strong thermometamorphic imprint generated by Mt. Capanne monzogranite and the pervasivity of the D_2 structures obliterate most of the blastesis/deformation textures associated to D_1.

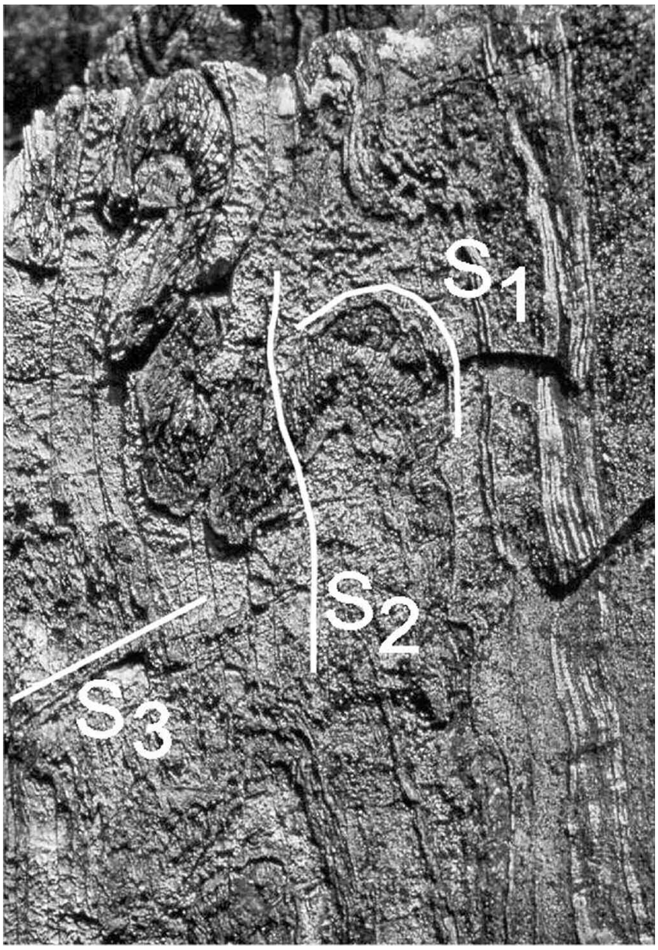

Fig. 3 - Isoclinal F_2 fold refolding S_0//S_1 and cut by C_3 fracture cleavage in the metalimestone (Casa Peria area, between Chiessi and Colle d'Orano); note the cleavage refraction of S_2 in correspondence of the cherty layers.

D_2 is associated to the most evident folding structures of the metamorphic aureole and is pervasive on the D_1 structures (Plate1f, g and Fig. 3). D_2 structures are characterized by centimetric to metric, non-cylindric, close to isoclinal folds with evident asymmetries. The hinge line generally curves up to a sheath fold geometry e.g., in the Spartaia-Marciana (see also Daniel and Jolivet, 1995) and in the Cavoli-Colle Palombaia (see following paragraph) outcrops (locations in Fig. 2). Locally sharp angular hinge zones occur as in the chevron folds within the chert outcrops of Spartaia and the neighbor Isola Paolina. The geometry of these folds is generally of similar-type and fits in the divergent, parallel and convergent isogons fields (1C, 2 and 3 classes) according to Ramsay's (1967) classification.

The S_2 axial plane foliation is pervasive at every scale and it is characterized by discrete and subordinately zonal crenulation cleavage that is spaced at mm-cm scale. In any case, a main composite S_1//S_2 foliation is generally recognizable along the F_2 limbs and represents the main schistosity of the rocks (Plate 1g and Fig. 3). Cleavage refraction phenomena (cm in size) are peculiar in some outcrops, in correspondence of cm/dm alternations of lithotypes (Fig. 3). It is evident that part of the contact blastesis is syn-kinematic with respect to S_2.

The distribution of F_2 axes orientations is generally subparallel to the pluton-host rock contacts as shown by the data of the stereonets (Fig. 4) obtained for the different parts of the metamorphic aureole and summarized in Fig. 5. The F_2 axial planes generally dip at intermediate angles towards the outer part of the thermo-metamophic aureole (Fig. 4), but they can vary their inclinations (up to sub-vertical) within a few tens of meters. Also the intersection lineations between S_0//S_1 and S_2 are congruent with the above-mentioned axes distribution being substantially parallel to the contacts with the pluton (see Principi et al., 2015b).

D_3 The D_2 structures have been locally bent by the subsequent non-metamorphic D_3 folding event. The F_3 folds are open- to close-type and metric to decametric in size; their hinge zone is always curved and the axial planes show a low-angle inclination (see Figs. 3 and 5 in Coli and Pandeli, 2001). Their geometries are in the fields with divergent, parallel and convergent isogons fields (1B, 1C and 2 classes) according to Ramsay's (1967) classification. The distribution of their axes orientations in the different parts of the metamorphic aureole is rather similar to those of F_2 (cfr. Figs. 4 and 5). Zonal crenulations and/or fracture cleavages, locally filled by hydrothermal mineralizations, are associated to F_3 (Fig. 3).

Syn-metamorphic shear zones

Shear zones are often reported in the surroundings of the contact between host rocks and plutonic bodies (e.g Costamagna et al., 2016). Ductile shear zones of different thickness (from decimetric to decametric) are present within the contact aureole of the Mt.Capanne pluton (see also Daniel and Jolivet, 1995). Two examples of shear zone are recog-

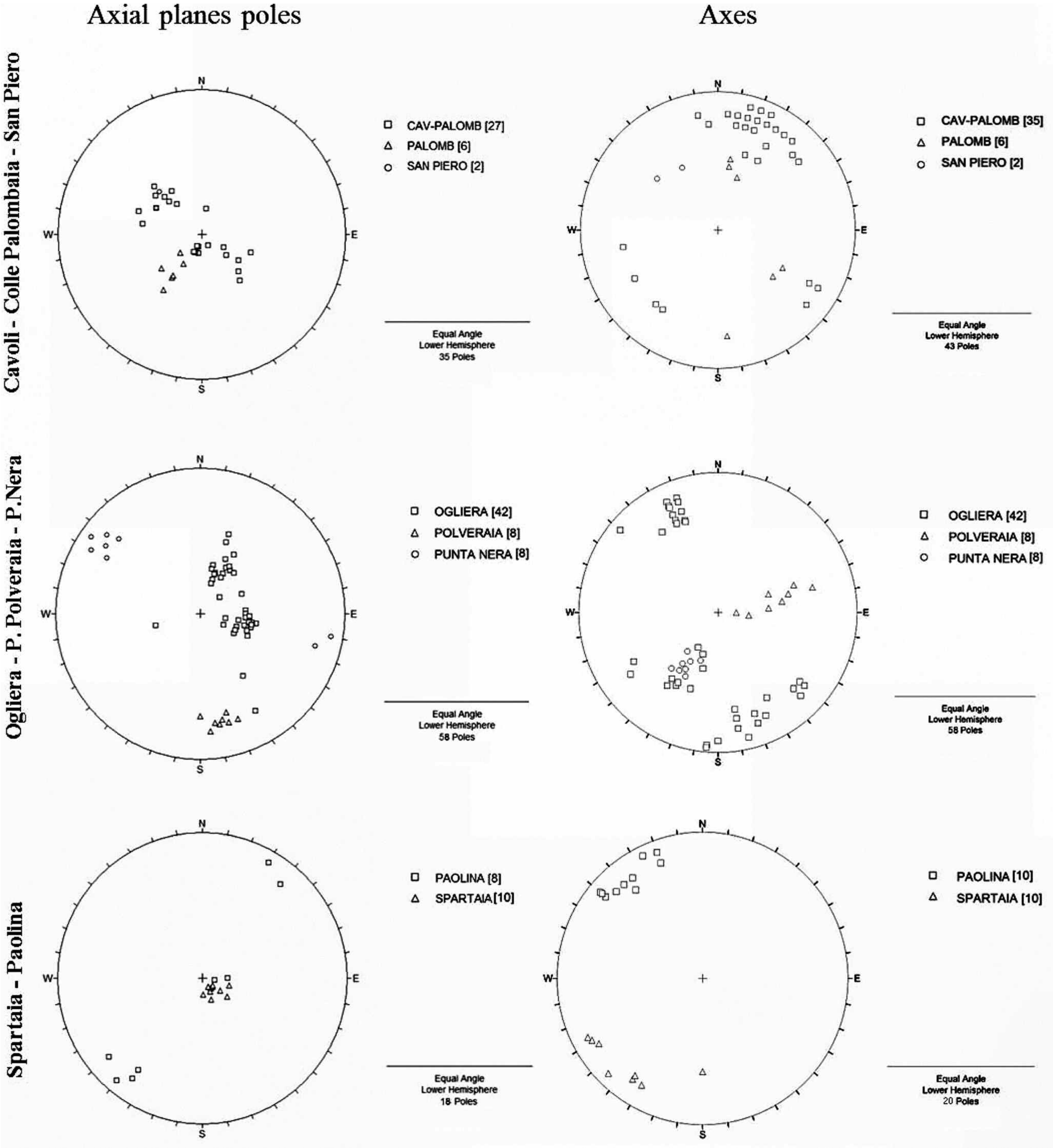

Fig. 4 - Stereonets (Schmidt stereonet, lower hemisphere) of the F_2 axial planes and axes in the PFU rocks in different zones of the metamorphic aureole.

nizable in the metalimestones of the Spartaia and Cavoli-Colle Palombaia outcrops (locations in Fig. 2). These shear zones are interkinematic between the D_2 and D_3 event, in fact, the metamorphic minerals lying on the S_2 are locally deformed by the shear zones and finally by S_3 non-metamorphic folds.

a) Spartaia.This shear horizon is located along the coastal path west of the Spartaia Bay. Here the alternating foliated marbles and calcschists of the metalimestones are deformed into metric-decametric, tight to isoclinal folds, referable to F_2 (see previous paragraph), that are characterized by a millimetric to centimetric-spaced axial plane foliation (Fig. 6) and by a mainly NE-SW and NW-SE axial strike and a northern dip (Figs. 4 and 5). F_2 deformed a previous metamorphic layering (S_1) which corresponds to the lithological alternance. Some whitish metaporphyries cut the $S_0//S_1$ surface of the metacarbonate beds and are often parallel to the limbs and axial plane of the main F_2. The former are affected by D_2 folding and shearing together with the host marbles and, particularly, S_2 cuts the contacts between host metacarbonates and metaporphyries (see magnifications in Fig. 6 and photomicrograph of the foliated dike in Plate 2m). HT metamorphic minerals (see Tab.5) locally grow along S_2 also as foliation-parallel veins and/or are static-mimetic with respect to the foliation. Ves, Grs and Wo also fill veins between the metapelitic boudins, with sub-vertical attitude with respect to $S_1//S_0$. Finally hydrothermal minerals (e.g. Ep, Qz) are associated to later (post-D_2) centimetric to decimetric - spaced fractures.

b) Cavoli - Colle Palombaia. In this area, we studied in particular sites 1 and 2 along the panoramic road (Figs. 7a and b) and site 3 in the westernmost cliff of the Colle Palombaia beach (Fig. 8). These sites can be considered as belonging to a main Cavoli - Colle Palombaia shear zone. In all these outcrops the meta-limestones show mylonitic structures associated to ductile shear zones. The dip of the mylonitic foliation is generally towards SE (that is parallel to the axial plane foliation of F_2, see Fig. 7a) and the senses of shear inferred by kinematic indicators (e.g., σ- and δ-type porphyroclasts, asymmetric folds) highlight the presence of a single tectonic transport direction that is outwards with respect to the Mt. Capanne intrusive massif (see below).

In the Sites 1 and 2 the decimetric up to some meter thick shear horizons are made up of Cpx- and Wo-bearing marbles and are pervasively foliated and characterized by enclaves and pods (i.e. rigid markers) of other lithologies like meta-pelite and fine-grained metacherts that are aligned along the mylonitic main foliation.

In site 1 (Fig. 7a) the XZ plane of the mylonitic horizon shows an average dip direction of 140° to 160° with a dip of 35° (140-160°/35), while the YZ plane lies in a NE-SW direction. The mineralogic lineation (= Lm, on the XY strain plane) has a plunge towards 165°. In site 2 (Fig. 7b) the main foliation has a dip direction 175-265°/30°, whereas Lm has a mean plunge of 240°/25°. The angular difference between the foliation and Lm strike is not more than 20°.

In both sides, the mylonitic foliation is mainly made up of Cal, Bt, Ms, Qz, Amp, Wo, Cpx. The kinematic indicators (e.g. σ- type And porphyroclasts in Plate 2f), present along the mylonitic foliation, point to an overall top-to-the-SE component of shear).

Some of them are elliptical pods that can be classified as quarter mats/quarter folds (Passchier and Trouw, 1996), showing a symmetrical morphology, with long axes parallel to S_2 on the XZ plane and a circular shape on the YZ plane, defining a prolate-type ellipsoid in 3D (Fig. 7). The distribution of the ellipsoids of the pods on the XZ plane show different trends, and the outcrop can be divided in three parts (see sketchs and closeups in Figs. 7a and b): two of them are characterized by an asymmetrical arrangement (i.e. simple shear deformation) and the central one shows instead a symmetrical setting (i.e. pure shear deformation). So it is evident the coexistence of coaxial (pure shear) and non-coaxial (simple shear) deformations in the mylonitic horizon. Different fold structures are present in the outcrop: sheath folds for non-coaxial strain parts and similar folds in the coaxial strain parts (Fig. 7a) and the mylonitic S_2 foliation is the axial plane foliation of these folds.

In the Site 3 (Figs. 8a - e), the thickest (max 10 m) ductile shear zone recognized so far in the thermometamorphic aureola as a whole is exposed. In fact, this mylonitic zone is about 10 m and at least some dam in lenght. The attitude of the mylonitic foliation has a dip direction 95°- 185°/30°-45°. Here too, Lm lies on the main foliation plane.

Numerous heterometric (from a few millimeters to more than 1 m in size) rigid markers or pods of metabasalts, metacherts and metapelites are present in the mylonitic marble (Fig. 8a). A noteworthy variability of the strain distribution

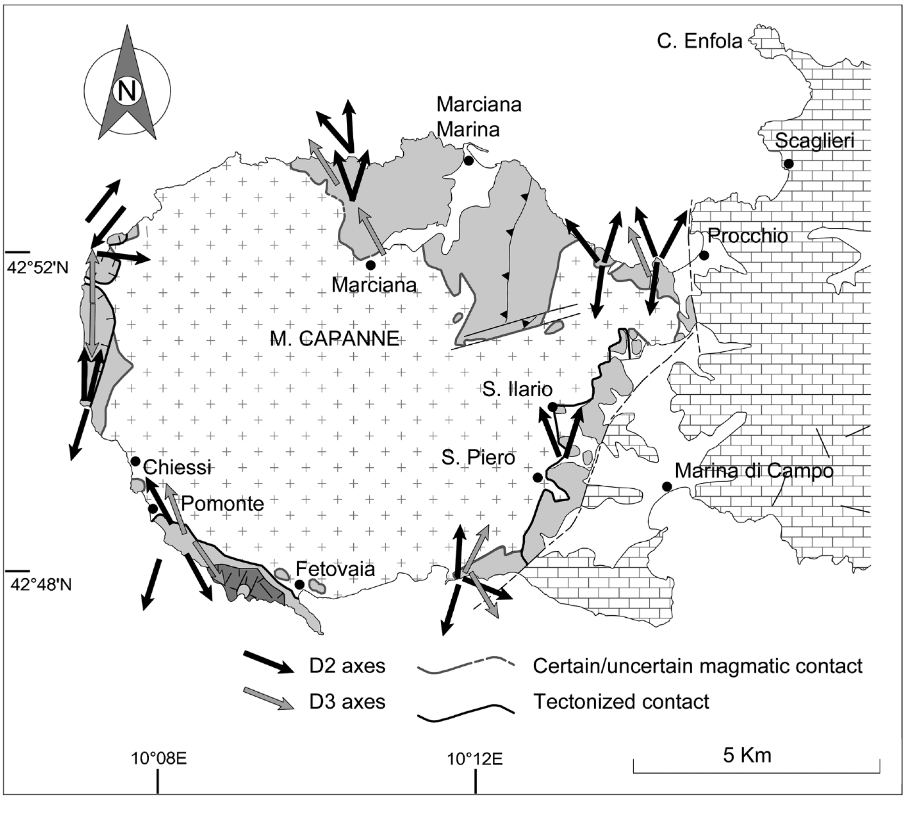

Fig. 5 - Areal distribution of the main attitude of the F_2 and F_3 axes in the Mt. Capanne metamorphic aureole and nature (i.e. intrusive or tectonic) of the contact between pluton and hornfels. The geological legend is the same of Fig. 2.

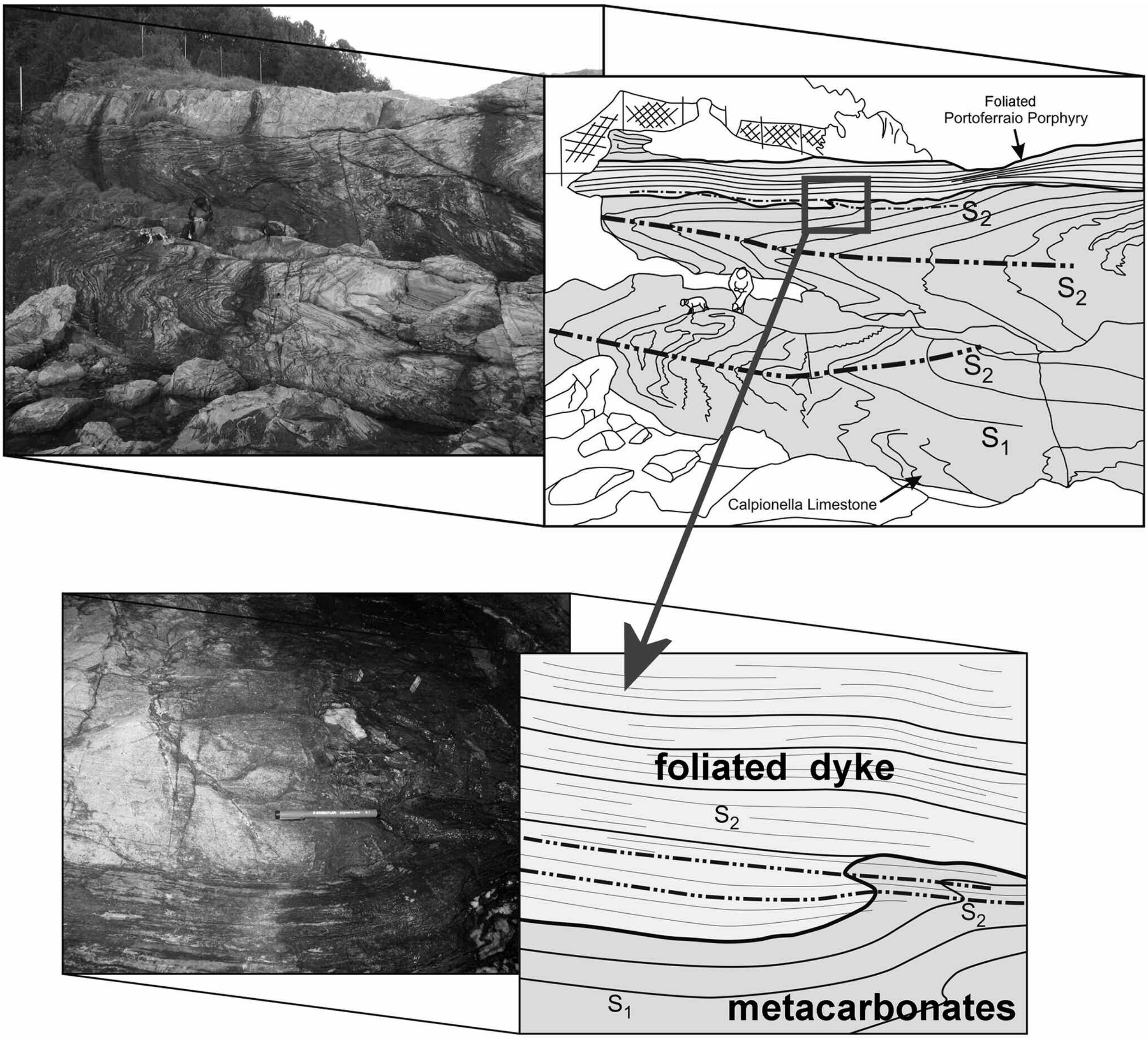

Fig. 6 - Structural features of the Spartaia shear zone. Folded metalimestone including a foliated Portoferraio-type metaporphyritic body (modified from Pandeli et al., 2013).

is shown in Fig. 8b. In particular, coeval simple and pure shear deformations coexist: the two pods reacted differently to stress. In the case of pod 1(sx), pure shear prevailed (mild back rotation), in the case of pod 2 (dx) simple shear dominated (forward rotation, comparable with Fig. 4a in Xypolia, 2010). This setting evidences general shear conditions in which several markers that differently react to the stress, in spite of maintaining the same shortening and extension directions. Moreover several kinematic indicators (e.g. mantled porphyroclasts, domino-type structures, boudinage), are present in this broad outcrop and allow to define a general top-to-the-SE sense of shear (Figs. 8b - e). The mylonitic foliation is weakly deformed by later open folds at the outcrop scale and is crossed by spaced middle-angle joints filled with hydrothermal minerals (e.g. Cal ± Tre/Act, Fig. 8d).

Vorticity analysis

Given the high quantity of kinematic indicators in the Cavoli-Colle Palombaia mylonitic shear zones, characterized by general shear, we could apply the kinematic vorticity (W_k) analysis to better define the deformative conditionsthat W_k is a dimensionless measure of the rotation relative to strain. This parameter characterizes the amount of shortening proportional to displacement and it is essential for the complete understanding of flow in ductile shear zones (Forte and Bailey, 2007). It is obtained through the analysis of elliptical objects (porphyroclasts) rotating in a fluid matrix, for the characterization of shear zones in different geodynamical context (Klepeis et al., 1999; Xypolias and Koukouvelas, 2001; Bailey and Eyster, 2003; Law et al., 2004; Jessup et al., 2007; Xypolias, 2010). Accordingly, W_k shows the relative rate of pure and simple shear in the flow deformation ($W_k = 0$ for pure shear and $W_k = 1$ for simple shear, Simpson and De Paor, 1993). We used two graphical methods (RGN and PHD with average error about 10%, Forte and Bailey, 2007) for the definition of W_k or better its

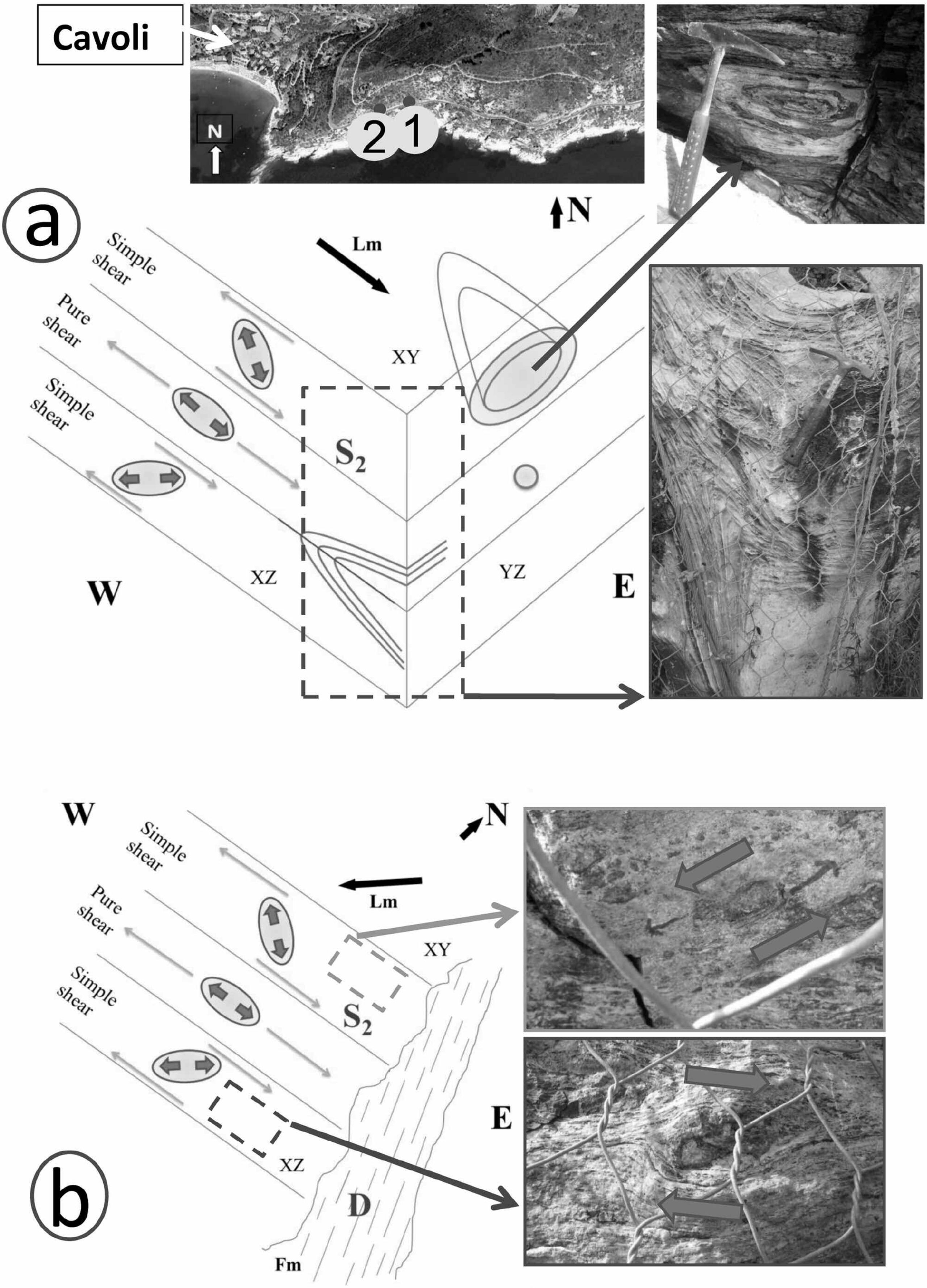

Fig. 7 - Structural features (closeups of the outcrops and sketchs of their structural interpretation) of the mylonitic shear zones along the panoramic road between Cavoli and Colle Palombaia: (a) site 1- similar-type and sheath-type folds; (b) site 2- Rotated pods and mantled porphyroclasts (grey or blue arrows in b/w and in colour texts, respectivelly = sense of shear). The sketches are not in scale. The locations of the sites 1 and 2 are in the panoramic picture respect to Cavoli.

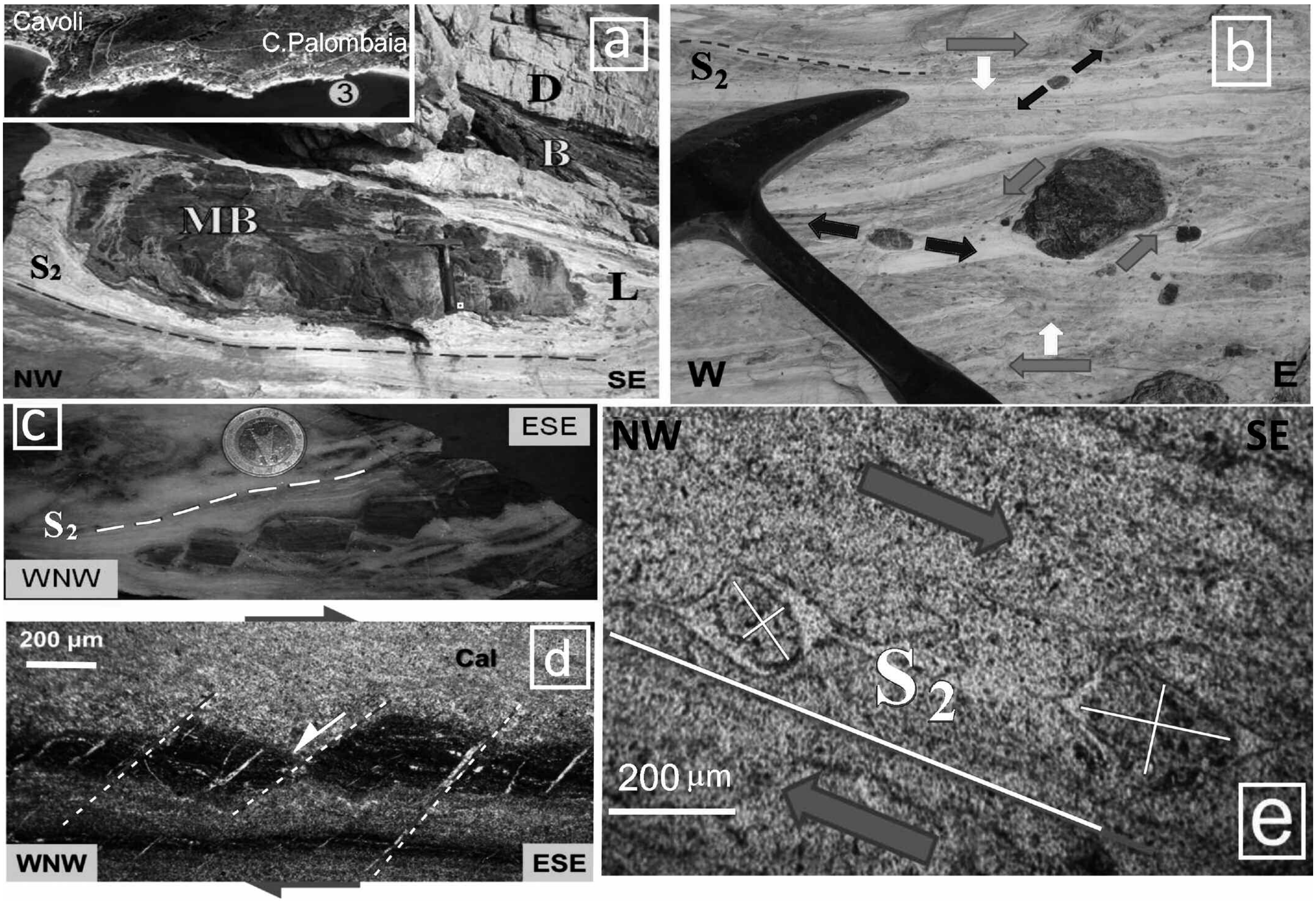

Fig. 8 - Structural features of the mylonitic shear zones in the western part of the Colle Palombaia beach (site 3). a) outcrop of the mylonitic horizon: C- metachert, B- metabasalt, MB- metabasalt megapod, L- mylonitic metalimestone; b) partitioning of simple and pure shear in the mylonite as evidenced by deformed pods (white or orange arrows in b/w and in colour texts, respectivelly = shortening direction; grey or blue arrows= sense of shear; black or green arrows= extension direction); c) and d) domino-type structures at the meso- and microscale of metapelitic boudins within the mylonitic metalimestone; e) example of rotated porphyroblasts utilized for defining the kinematic vorticity (grey or blue arrows in b/w and in colour texts, respectivelly = sense of shear). The location of the site 3 is in the panoramic picture of the Cavoli-Colle Palombaia area.

average value (W_m) in the mylonitic horizon of the Colle Palombaia beach, measuring the θ angle between the long axis of the porphyroclast and the main foliation both in the outcrops of the three sites and at the microscopic analyses through thin sections analysis (see Fig. 8e). In particular:

1) the Rigid Grain Net method (RGN, Jessup et al., 2007) (Fig. 9a), allows us to plot on a bivariant diagram a couple of values measured for each porphyroclast, the θ angle and the shape factor B*,

$$B^* = \frac{(M_x^2 - M_n^2)}{(M_x^2 + M_n^2)}$$

where M_x and M_n are respectively the long and the short axis of the clast. The W_m value is directly inferred from the plot, in correspondence with a cut-off point or interval, dividing the field of infinitely rotating particles from that of stable particles;

2) the Porphyroclast Hyperbolic Distribution method (PHD, Simpson and De Paor, 1993) (Fig. 9b) uses only two parameters that are the axial ratio (R = long axis/short axis) and θ. R and θ are then plotted on a hyperbolic net (De Paor, 1988) along with shear sense, using symbols to distinguish back- and forward-rotated grains. The cosine of angle, related to inclined eigenvector (ν) that enclosing the field of back-rotated grains, is then used to calculate W_m (W_m = cos ν, Simpson and De Paor, 1993).

W_k values were defined in the studied outcrops for both the rotated porphyroclasts and are shown in Figs. 9 a and b with different colors: data from sites 1 and 2 in green, data from site 3 in red and data from thin sections in blue (related to the 3 sites). Both RGN and PHD methods (Figs. 9a and b) point out similar results for W_m (0.675-0.72 and 0.707 respectively), highlighting the congruence between field data (meso-scale) and thin section analyses (micro-scale). Therefore, the data range is consistent with the general shear regime (Fig. 9c).

Brittle structures

Two main types of brittle structures are present:

1) Low- to medium angle faults. Two of them are well recognizable at the cartographic scale (see Figs. 1 and 2 and Principi et al., 2015 a; 2015c): 1) The FF Fault that allows the superposition of the non-metamorphic PTU above the hornfels of the PFU Unit (it is noteworthy the small tectonic window close to Punta Le Tombe; 2) the doubling tectonic surface that is present within the PFU in the western part of the aureole that superposes a "complete"-type succession

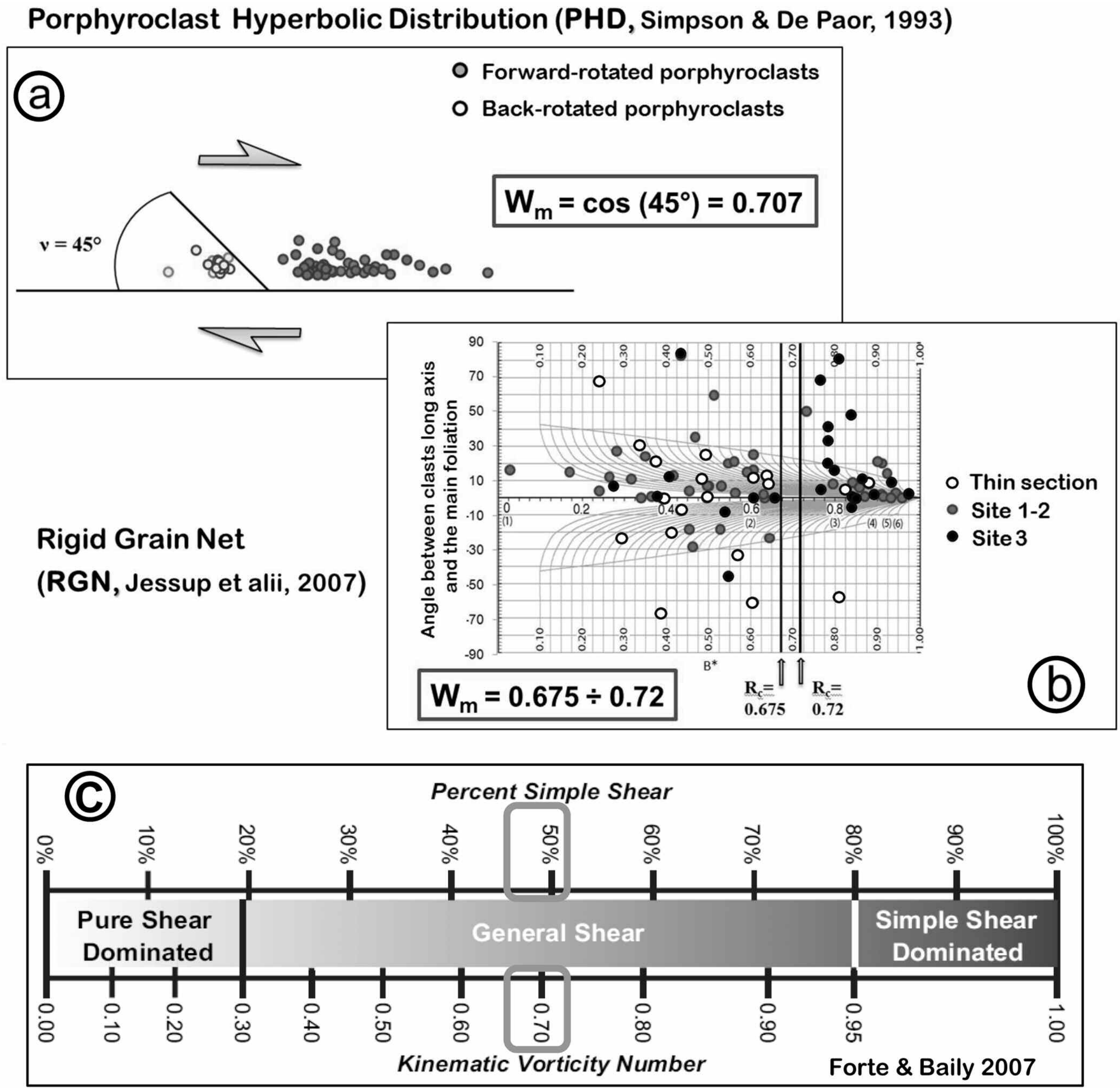

Fig. 9 - PHD (a) and RGN (b) kinematic vorticity diagrams for the data collected in the Cavoli-Colle Palombaia sites and plot of W_m in the scheme of simple shear vs. kinematic vorticity (c).

above the "reduced"-type, metapelitic-rich one (in intrusive contact with the pluton) and the pluton itself. This tectonic surface is locally underlined by cataclastic breccias e.g. in the outcrops east of Punta Polveraia.

Other low-angle fault surfaces are recognizable in other parts of the metamorphic aureole, locally also close to the contact with the underlying pluton. It is the case of the S.Piero area where it is evident a "jump" in metamorphic zoning (the medium-low grade facies hornfels are in contact with the pluton, see Discussion) and centimetric to decametric-sized striations and stretching lineations at the top of the pluton that point to a top-to-the-E /- ESE sense of shear (see also Daniel and Jolivet, 1995).

2) High-angle faults and jointing. The contact metamorphic rocks of the aureole, as well as the granitoid, are also affected by fracturing and faulting. The average strikes of the main fracture systems in different part of the metamorphic aureole are shown in Fig. 10. Their comparison with the fracture distribution observed in the pluton and that of the later Orano Porphyry dikes, reveal similar trends in the different parts of the metamorphic aureole (Figs. 1, 2 and 10). A more detailed survey of the fracture systems was performed in the Colle Palombaia area and in the S. Piero quarries.

The stereonets of Fig. 11 show: 1) the strike of fractures in the Mt. Capanne granitoid that reveal two main trends, one about NNW-SSE (with a NE-SW directed secondary system) and the other about NE-SW (with an about E-W directed secondary system). The first one (with a radial attitude respect to the pluton dome) is dominant in the Colle Palombaia area, whereas the second one (parallel to the plu-

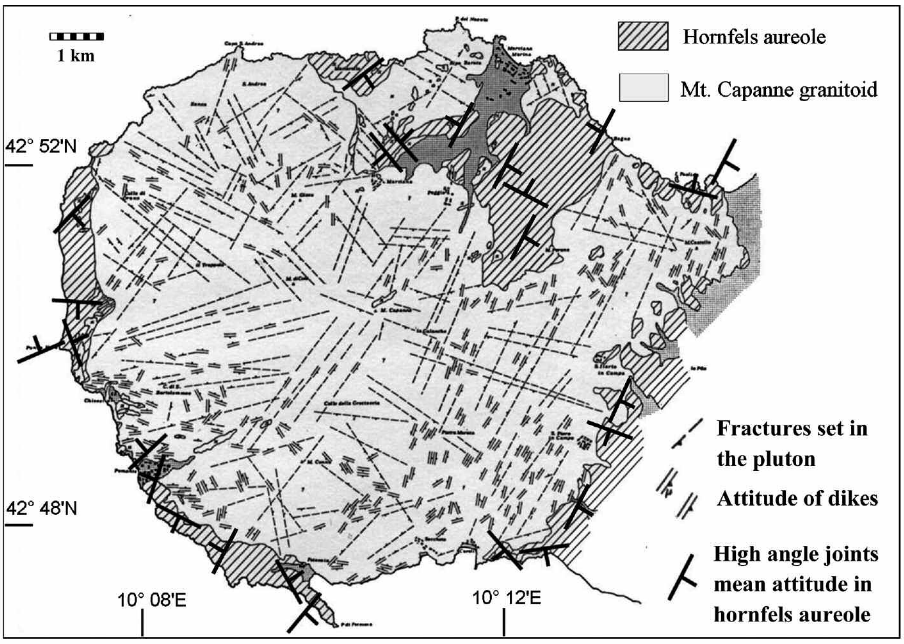

Fig. 10 - Main attitude of the joints in the contact aureole in different areas (our data) and in the pluton (modified from Boccaletti and Papini 1989).

ton boundary) is the main system in the S.Piero quarries. ENE-WSW striking fractures (with a NW-SE directed secondary system) prevail in the host PFU rocks at Colle Palombaia (Fig. 11). Finally the EBF composite high-angle normal Fault, characterized by segments with an overall NE-SW and N-S strike, downthrows CU with respect to PFU towards east (Figs. 1 and 2).

DISCUSSION

The data shown in the previous chapters refine the stratigraphic, petrographic and structural model of the whole aureole of the Mt. Capanne intrusive body and about the Late Miocene to Pliocene deformation and metamorphic history of tectonic units in the Elba Island.

Stratigraphy

Despite of the locally strong metamorphic imprint, the lithological associations of PFU can be correlated to a original "typical" ophiolitic succession (see Fig. 2b) that appears similar to that of the OU cropping out in eastern Elba (Principi et al., 2015a; 2015b) and, more in general, to those of the continental Northern Apennines (i.e Vara Unit in Tuscany and Liguria: Bortolotti and Principi 2003; Marroni et al., 2004; Nirta et al., 2005). In fact, the PFU lithotypes associations can be correlated to the following formations of the Vara Unit (from the bottom): Serpentinites, Ophiolitic breccias, Gabbros, Basalts, Monte Alpe Cherts, Calpionelle Limestones and Palombini Shales. In agreement with (Spohn, 1981), the peculiar metapelitic-metasiltstones dominant assemblage of the Marciana area in the upper part of the PFU could be correlated to Lavagna Shales-type sediments that rests at the top of the Palombini Shales in the Vara succession of eastern Liguria. The age is Aptian-Cenomanian for the finding of microforaminifera in the Fetovaia Promontory by Bouillin (1984).

In addition, in PFU we recognized at least three sub-units: 1) the "complete"-type sub-unit, that represents most of the outcrops of the metamorphic aureole, geometrically overlies two "reduced"-type sub-units that are in intrusive contact with the pluton, i.e 2) consisting only of meta-Palombini Shales including basaltic bodies in the Punta del Timone-east Punta Polveraia area and 3) represented by Serpentinites + Gabbros in the Mt. Perone-Bagno areas. In this framework it is possible the correlation of sub-unit 1) with the Volterraio sub-Unit, of sub-unit 2) with the Acquaviva sub-Unit and of sub-unit 3) with Sassi Turchini sub-Unit in the OU of eastern Elba (see Fig. 22 in Principi et al., 2015b for the different sub-Units in OU). Regarding the contact of sub-units 1) and 3), it resembles the tectonic superposition of the Volterraio sub-Unit above the Sassi Turchini sub-Unit. Instead, we interpret the contact of sub-units 1) and 2) as due to the Late Miocene detachments during uplift of the pluton, but a remobilization of an older thrust surface cannot be excluded.

However, the direct correlation of the PFU successions with the OU sub-units of eastern Elba is hampered by the apparent absence in the 1) "complete"-type sub-unit of the mainly marly Nisportino Formation that characterizes most of the OU sub-units (i.e. Bagnaia, Volterraio and Monte Serra sub-Units) at the transition between Monte Alpe Cherts and Calpionelle Limestones (Bortolotti et al., 1994b). In spite of some horizons of calcschists are present within and close to the base in the metalimestones of the Procchio-Spartaia outcrops and calcareous siliceous levels can be locally recognized in the meta-cherts, a true thick transitional formation seems to lack in the PFU.

As previously said, some authors (e.g. Perrin, 1975; Reutter and Spohn, 1982; Coli and Pandeli, 2001) proposed correlations of the ophiolitic successions of the Mt. Capanne thermometamorphic aureole to the *Schistes Lustrés* of Alpine Corsica. Ophiolitic sequences lithologically similar to those of the Elba Island are in fact present in NE Corsica both in the *Schistes Lustrés* and in the non-metamorphic ophiolitic successions of the Balagne Unit (Durand-Delga, 1978; Durand-Delga, 1984; Marroni et al., 2004; Molli, 2008). The *Schistes Lustrés* are also present in the Tuscan Archipelago and along the Tuscan coast (Gorgona Island, Rossetti et al., 2001 and Orti et al., 2002; Giglio Island, Rossetti et al., 1999; Argentario Promontory, Elter and Pandeli, 2002) and show a typical high pressure/low

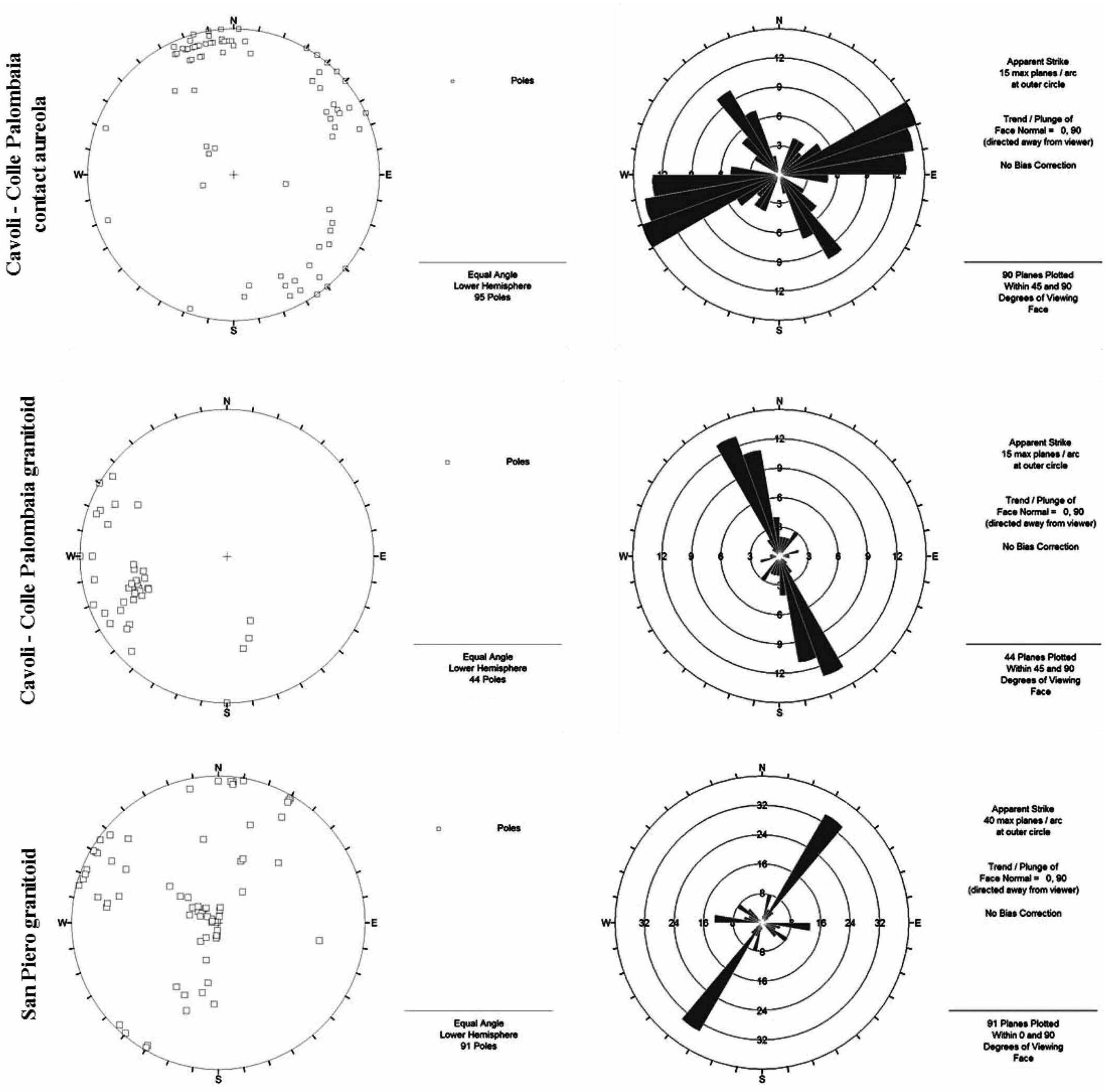

Fig. 11- Stereonets (Schmidt stereonet, lower hemisphere) and rose diagrams of the attitude of joints at Colle Palombaia (both in the contact aureole and in the granitoid) and at San Piero (in the granitoid).

temperature metamorphic imprint related to the Cretaceous-Eocene to Oligocene subduction of the Ligurian-Piedmontese oceanic lithosphere (Jolivet et al., 1998; Brunet et al., 2000). *Schistes Lustrés*-type rocks were identified by previous authors in eastern Elba (i.e. Acquadolce Unit, Bortolotti et al., 2001a; Pandeli et al., 2001a), where Bianco et al. (2015) recently found HP-LT minerals, but these minerals are not present in the studied samples of the PFU. Their lack may be due to obliteration by the subsequent contact metamorphism of the Mt. Capanne pluton, but they were not found in the very low grade hornfels facies (e.g. Fetovaia Peninsula) either. Thus, the attribution of PFU to OU or to the Vara Unit, instead than to the *Schistes Lustrés*, is more probable.

Metamorphic zonation

The contact metamorphism zonation in the different outcrops of Mt. Capanne (Figs. 12a, b, c) was defined on the basis of the hornfels facies (e.g. Turner, 1981; Kerrick, 1991; Bucher and Frey, 1994; Winter, 2010; Bucher and Grapes, 2011): the Ab-Ep facies (low grade), the Hbl facies (medium grade) and Px facies (high grade).

Hornfels of medium to high grade are generally recognizable in the aureole with PT conditions of T 3[illegible]°C and P = 1,5-2 kb.

In particular, the low- to very low- grade hornfels are represented only in the Punta Fetovaia, in the Ogliera-Pomonte, in the San Piero-Sant'Ilario and Marciana Marina-

Bagno areas (see Fig. 12; locations in Fig. 2). The highest metamorphic grade in the Px facies was found in the recrystallized Monte Alpe Cherts, Calpionelle Limestones and Palombini Shales, of several places (see Fig. 12 and Tables 4, 5, 6). In particular, a mineral association of Cal + Grt(Grs-Adr) + Cpx + intermediate to calcic Pl ± Bt ± Qz ± And is mostly present in the metacarbonates of the Calpionelle Limestones, but also Ves + Wo + Kfs ± Sc p ± Ms often occurs (e.g. in the Cavoli-Colle Palombaia, Marmi, Procchio-Spartaia and Marciana-Marciana Marina).

In some outcrops (e.g. Cavoli-Colle Palombaia, Spartaia-Punta Agnone), the marbles can be locally completely transformed into a Wo + Cpx(Di) skarn. Similar mineral associations (with rare Scp) are present in the metalimestones of the Palombini Shales cropping out in the western part of the aureole between Chiessi and Punta Polveraia, but also in the Spartaia, Marciana and Fetovaia areas. The transformation of the metacarbonate rocks into skarn bodies (e.g. the skarns at Spartaia-Punta dell'Agnone) was due to metasomatic replacement of Cal with calc-silicates (e.g. Grt, Cpx and Wo) through decarbonation reactions driven by upflowing magmatic fluids (cfr. Rossetti et al., 2007). The metapelitic intercalations are instead characterized by Bt + Cpx + Cal + anortitic Pl + Crd + Kfs ± Scp.

Considering also the muscovite breakdown and the decarbonation reactions, these mineral associations points to peak T of about 600-620°C for 1.5-2 kb (Johnson et al., 2000; Bucher and Grapes, 2011; Buriánek and Dollniček, 2011; Casillas et al., 2011) up to 650-670°C (Winkler, 1979; El Khalile et al., 2014). Taking also into account the $X(CO_2)$ proposed by Rossetti et al. (2007) and the Qz-free HT mineralogic assemblages, a T peak > 610°C can be inferred for these PFU rocks. It is noteworthy that the presence of Scp (also in veins parallel and perpendicular with respect to the main HT foliation) is only in connection with Ms-and Qz-free, higher grade hornfels and skarn mineral associations (e.g. Ves + Grt + Cpx + Wo + anortitic Pl ± Kfs, in the brown-green contact horizons of the hornfels with the pluton). The presence of Hc + Mnz in the And ± Cpx + Grt(Alm) + P ± Crd(± Ms ± Qz) mineral association defines the higher metamorphic grade in the Monte Alpe Cherts of the Colle Palombaia area and suggests for them temperature perhaps close to 700°C (Bucher and Frey, 1994; Bucher and Grapes, 2011). Hercynite was also found within the mafic micro-granular enclaves in the Sant'Andrea facies of the Pluton (Gagnevin et al., 2004). Therefore T exceeding 650°C can be hypothesized for the highest thermal peak conditions that occurred in the aureole. Anyway, given that there is no evidence of melting in the hornfels rocks, temperature cannot have exceeded the melting reaction.

The meta-ultramafic and metabasitic rocks are generally in the Hbl hornfels facies also where they are in contact with the pluton or are associated to metasedimentary successions characterized by Px hornfels facies. Only the disappearence of serpentine in the Ol (neoblastic) + Tr + Hbl + Tlc association of the meta-serpentinites and the presence of calcic Pl blasts in the metagabbros and metabasalts suggest the passage to a higher grade at the Chiessi-Punta Polveraia, Cavoli-Colle Palombaia and Mt. Perone sites (Figs. 12a, b).

The distribution of metamorphic grade in the different protoliths (ultramafic + basic magmatic vs. sedimentary) in the same outcropping area, first suggests that the thermal flow produced different metamorphic imprints in the different lithotype assemblages, even where at the same distance from the contact with the pluton. In this framework the

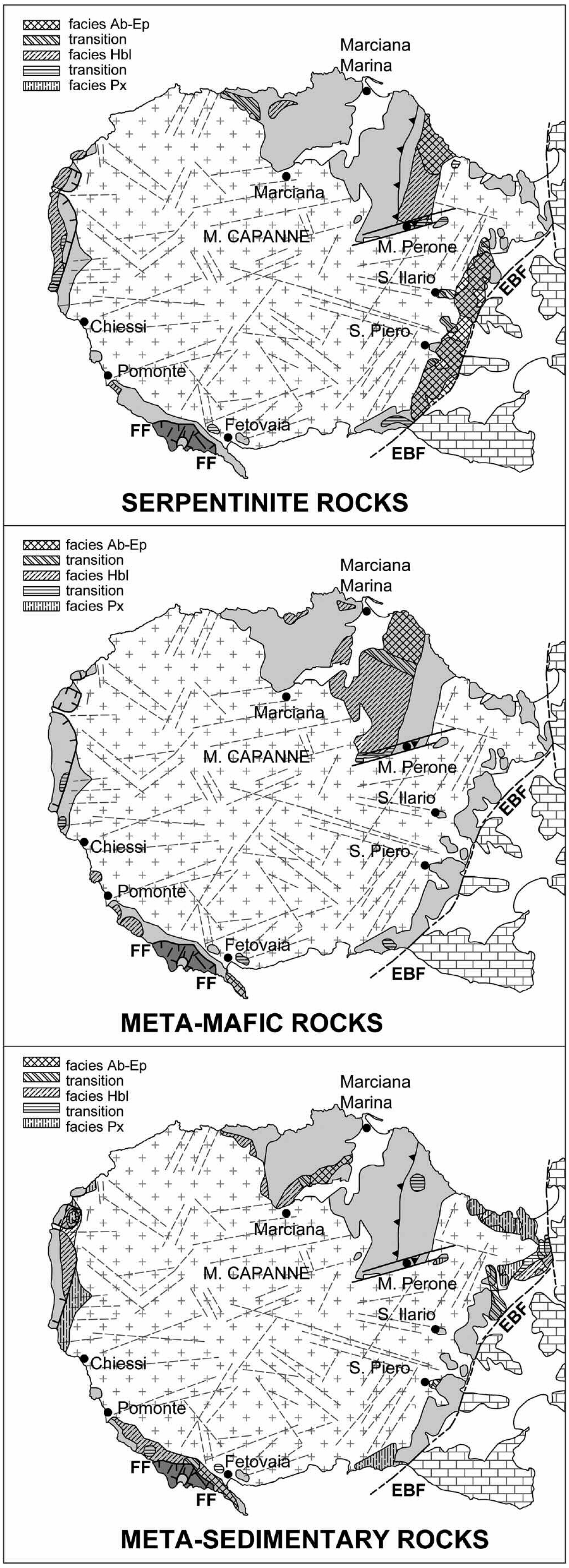

Fig. 12 - Zonation of the hornfels facies in the Mt. Capanne aureole: a) serpentinite rocks; b) meta-mafic rocks; c) metasedimentary rocks. The legend of the geological units and the geographic references are those of Fig. 2.

metasedimentary lithotypes appear generally more sensitive respect to the magmatic metabasic and serpentinite ones. So, it is evident that the distribution of metamorphic facies and metasomatic effects in the Mt. Capanne aureole can be related not only to the distance respect to the pluton boundary. In fact, also to the physical features of the rocks are very important for the metamorphic zoning, e.g. the presence of primary and secondary anisotropies (e.g. bedding, foliations, fractures), which facilitated the circulation of hot fluids and, possibly, to the different thermal conductivity of the host lithotypes (e.g. limestones/cherts vs. basalts/gabbros or serpentinites).

Another important factor of variability was due to fracturing of the aureole rocks that occurred both during the pre-magmatic (i.e. orogenic) events and during the intrusion itself. In fact, in agreement with Rossetti et al. (2007), the local presence of HT minerals (e.g. Cpx, Ves, Wo, Scp)-bearing veins in the high grade metamorphic rocks suggests that the HT metasomatic fluids utilized joints (e.g. due to hydrofracturing, more developed in the bedded calc-silicate rocks with respect to the marbles) and previous structures (e.g. bedding, foliations) for their ascent during the contact event. These events produced a heterogeneous framework of fracturing and permeability in the host rocks during the emplacement and cooling of the pluton. Local preferential ways for the ascent of HT fluids are testified also by some "islands" of high grade hornfels within the overall low-medium grade assemblages, e.g. in the Pomonte-Ogliera area and south of Colle d'Orano (see Fig. 12c) that are linked to fracture systems that later were used also for the intrusion of aplitic to leucogranitic dikes.

The study of the distribution of the contact mineral associations in the whole aureole and the structural data show also that the primary contact of the pluton with the high grade contact facies is preserved in a few places (e.g. Cavoli-Colle Palombaia, Spartaia-Procchio-Marmi and Chiessi-east Punta Polveraia) (see Figs. 5 and 12). In the other part of the metamorphic aureole (e.g. San Piero-Sant'Ilario, south of Pomonte) the contact is clearly more or less reworked by detachment tectonics that allows the direct contact of low- to medium grade facies with the granitoid and locally shearing striations also occur at the top of the pluton (e.g San Piero area). In other places (e.g. north of Sant'Ilario, Maciarello-Marciana), the nature of the contact cannot be easily defined. Anyway, the thickness of the metamorphic aureole can be estimated in at least 150-200 m (see also the geological cross sections in Principi et al., 2015b and c; 300-400 m according to Bouillin 1983), as shown by the distance between the Grt-rich metalimestones of the Palombini Shales, at the contact with the pluton at the Fetovaia village, and the ~~same weakly~~ recrystallized formation in the Fetovaia Peninsula.

Most of the HT-LP minerals are syn-kinematic with respect to the axial plane foliation of the D_2 folds (e.g. in the Spartaia outcrops) and of the mylonitic horizons (e.g. in the Cavoli-Colle Palombaia area). However, the petrographic data suggest that the growth of the contact minerals occurred during a progressive history of deformation and metasomatic metamorphism, including (pre-)/syn- and post-kynematic events with respect to the development of S_2. In fact, some Wo and Cpx, Grt and And porphyroclasts appear rotated within the main S_2 foliation, generally as σ or δ-type mantled porphyroblasts. Moreover, Grt and vesuvianite porphyroblasts/-clasts can locally include Cpx and Wo blasts. Syn-intrusion hydrofracturing processes allowed crystallization of HT-LP minerals also in veins parallel to or crosscutting S_2 (see also Rossetti et al., 2007). Hydrofracturing processes were also described by Dini et al. (2008a) in the host rocks of the Porto Azzurro pluton in eastern Elba. In any case the presence of either static or mimetic growth of contact minerals is also observed for example as anhedral to sub-idiomorphic Grt or the Wo radiating spherules (sometimes with Di core and a fine-grained Cpx blastesis as rim). In other cases the spherules show an ellissoidic shape with their long axes parallel to S_2 and, at times, they are enveloped in this main foliation. This occurrence can be related to ductile vertical shortening processes (i.e. flattening) that suffered the PFU rocks during the "forced" intrusion of the pluton especially in its western parts, in agreement with Daniel and Jolivet (1995) (Fig. 13).

Finally, the twinning observed in the Cal blasts of the marble lithotypes are mainly of type II and, locally, of type III according to the scheme of Burkhard (1993), which indicates temperatures of 150 to 300° C. It is evident that these values are related to the shutdown temperature of the metamorphic system during the final stages of cooling of the pluton that shortly predate the development of high-angle fracturing. These data are in agreement with the temperatures of the hydrothermal mineralizations that fill the fractures: Qz + Ep(> 250°C), Qz + Adl ± Cal (230-250°C) and Qz + Chl + Cal (170-230°C) (cfr. Bertini et al., 1985; Ruggieri et al., 2006).

Structural synthesis

The collected meso- and micro-structural data, that are extended to the whole contact metamorphic aureole, refine the structural interpretation suggested by previous authors (Bouillin, 1983; Daniel and Jolivet, 1995; Reutter and Spohn, 1982; Bortolotti et al., 2001a; Coli and Pandeli, 2001; Pandeli et al., 2013). In particular, it appears evident that the rocks of PFU experienced a complex structural evolution that includes deformative events of different extent and nature and mostly related to the intrusion and exhumation of the Mt. Capanne pluton. Ductile deformations are well recorded in the metasedimentary formations, characterized by thin to medium-thick bedding and including carbonatic lithotypes, which developed polyphasic folding, i.e. the syn-metamorphic D_1 and D_2 events and a final D_3 event at the brittle-ductile transition. High-angle brittle fracturing and faulting followed, affecting also the pluton itself. The serpentinized ultramafic rocks as well as the massive basalts and gabbros are rarely interested by penetrative foliations and structures at the mesoscale. In most of the outcrops they appear only statically recrystallized by the contact metamorphism sometimes preserving textures originated during oceanic spreading (e.g. "flaser"-type texture of the gabbros, locally cut by unfoliated basaltic dikes in Plate 1b) that characterize most of the Ligurian successions of the Northern Apennines (see Cortesogno et al., 1975; 1987). In particular:

<u>D1</u> event is recognizable mainly in the fine-grained continuous S_1 foliation that is parallel to the bedding and forms the axial plane schistosity of rare unrooted isoclinal or sheath-type folds. No contact minerals are associated to S_1. Therefore, we think that D_1 event either occurred during a pre-Late Miocene shortening phase of the Northern Apennines tectogenesis or probably testify early ductile deformations connected to the beginning of heating and compression due to the "forced" Mt. Capanne intrusion, in any case before the main thermometamorphic recrystallization and the arrival of the HT metasomatizing fluids.

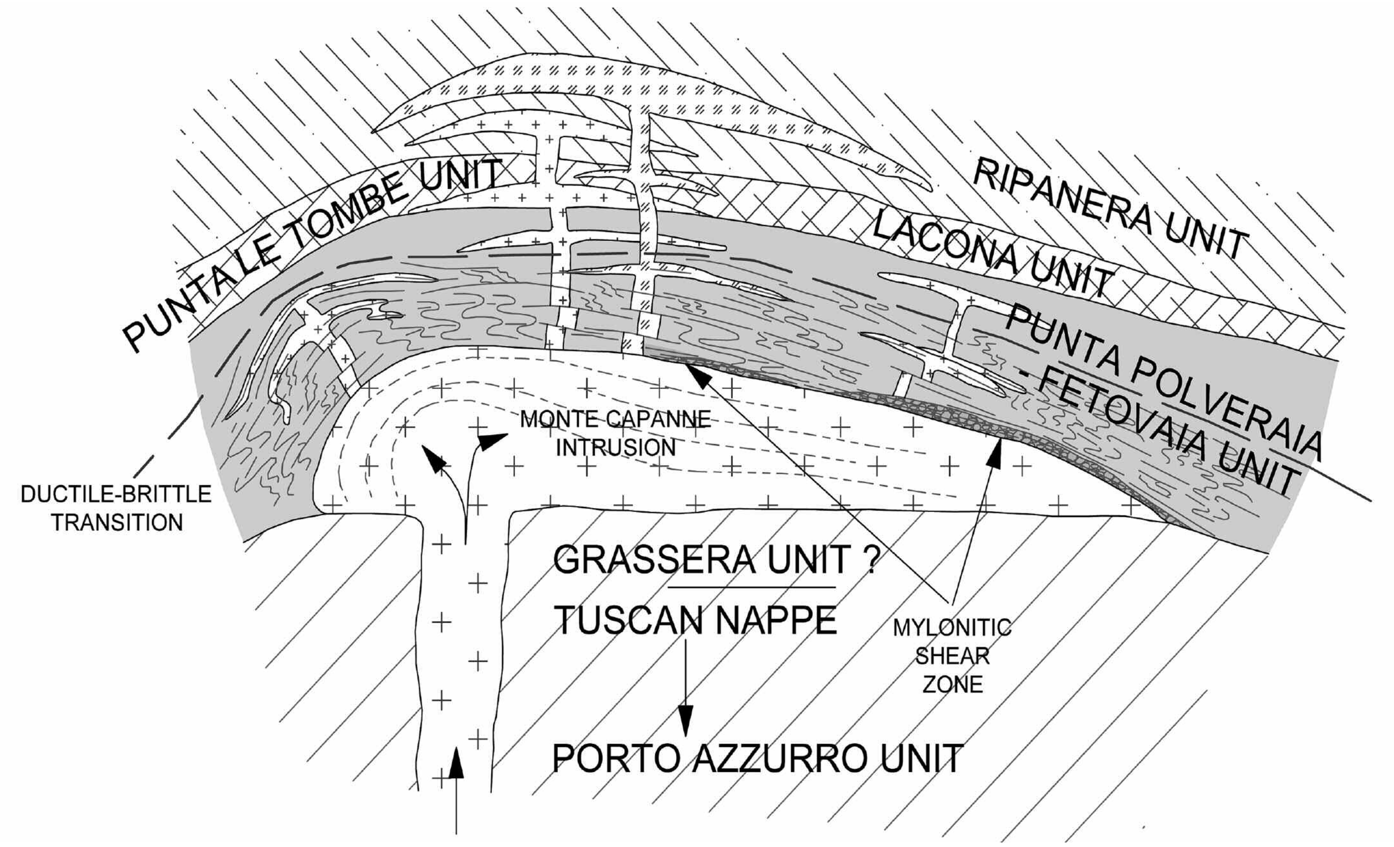

Fig. 13 - Sketch of the forced intrusion of the Mt. Capanne pluton and ductile deformations and shearing in the surrounding PFU successions (modified from Daniel and Jolivet, 1995).

D2 is the main folding event recognizable in the outcrops and at cartographic scale and is characterized by tight to isoclinal, non-cylindrical folds up to sheath fold in the more ductile and high metamorphic grade parts of the aureole (e.g. Cavoli-Colle Palombaia, Spartaia). Their axial plane foliation S_2 is a millimeter-centimeter scale, often discrete type crenulation cleavage, that is parallel to S_1 in the long limb of the folds producing the main very pervasive composite schistosity shown in outcrops. The contact metamorphic event appears coeval with D_2 folding because the growth of typical thermometamorphic mineral associations is along S_2 (e.g. Bt, Wo, Di) and given that the syn-D_2 deformation and metamorphism of PFU also affected the about 8 Ma Portoferraio Porphyry that intruded the ophiolitic succession (see the described shear band in the Spartaia area). Moreover, the orientation of axes, intersection lineations and planar elements of F_2 are substantially parallel to the contact of the aureole rocks with the Mt. Capanne Monzogranite. In addition, the axial planes generally dip towards the external part of the aureole. These data allow correlation of D_2 with the intrusion and ballooning phenomena of the pluton (Fig. 13). The variations over short distances of the dip (up to sub-vertical) of the F_2 axial planes can be related to following D_3 folding.

The eastward vergence of F_2 in the western part of the aureole (i.e. Pomonte-Ogliera and Punta Nera-Punta Polveraia (see also Reutter and Spohn 1982) seems in contrast with a simple radial folding around the rising pluton.

These folds allowed Reutter and Spohn (1982) to hypothesize that these structures were related to a “regional” metamorphic, Apennine-vergent orogenic event that pre-dated the Mt. Capanne intrusion. The syn-intrusive nature of the F_2 folds is testified by the sub-circular trend of the F_2 axes parallel to the pluton boundaries and their link with the contact blasteses showed in the previous paragraphs. This is a clear evidence that D_2 event is related to the pluton emplacement (Fig. 13, see also Daniel and Jolivet, 1995; Rossetti et al., 2007) and not to regional tectonic folding events that are characterized by NW-SE to N-S trending axes in the Elba Island and in the Northern Apennine chain (cfr. Elter and Sandrelli, 1995; Corsi et al., 2001; Principi et al., 2015a; 2015b). This hypothesis is also strengthened by the data on magnetic susceptibility anisotropies (AMS) collected in both the pluton and in the aureole rocks. In particular, Cifelli et al. (2012) showed a general correlation between the magnetic lineations in the hornfels with those obtained for the pluton by Bouillin et al. (1993) and its magmatic foliations, consisting in the orientation of Bt and Kfs megacrysts (Boccaletti and Papini, 1989; Farina et al., 2010). The correlation of the magnetic-magmatic lineation of the pluton with the syn-metamorphic stretching lineations and F_2 foliations of the host rocks suggests a common deformation history of the latter and the hot intrusive body. This is also in agreement with a ductile deformation of the aureole rocks along the entire perimeter of the ascending pluton rather than to regional deformation processes (see also Cifelli et al., 2012).

Despite the local variations of the attitude of the mylonitic foliations and of the mineralogic lineations in the same areas (likely due to the irregular shape of the top of the intrusive pluton), the kinematic indicators in the different decimetric to decametric shear horizons recognized in different part of the plutons reveal a general centrifugal tectonic transport with respect to the pluton and towards the external parts of the aureole as suggested also by the data on F_2 folds. This is substancially in agreement with the distribution of the mineralogic lineations shown by Bouillin (1983) and by Daniel and Jolivet (1995). The peculiar presence of stretching lineations characterized by a top-to the-east sense of shear also in the westernmost part of the aureole (Punta Nera-Punta Polveraia area, see also Daniel and Jolivet, 1995) is associated to a Miocene detached PFU sub-unit that had an original more eastern location with respect to the present. The finding of the decametric Colle Palombaia beach shear zones is particularly important also because the HT minerals lie along its main (S_2) mylonitic foliation and testify for the first time the presence of mylonites in the inner part of the aureole during the D_2 event that typically affected the very ductile Calpionelle-like marbles. Moreover, the presence of different shear regimes has been detected in the mylonitic horizons of the Cavoli-Colle Palombaia area owing to the both pure and simple shear structures in the same outcrop. Classically, the two shear deformation types are considered as exclusive, by using the concept of strain partitioning (linked to the different behaviour of heterogeneous lithologies), if found simultaneously in the same context. On the contrary, if we use the general shear model (Simpson and De Paor, 1993; Jessup et al., 2007) or the sub-simple shear one (Simpson and De Paor, 1993), the incompatibility of the two schemes can be overcome. In fact, this flow regime explains the simultaneous presence of translations and rotations. The kinematic indicators in the studied shear zones identify a deformation regime of general shear or sub-simple shear. This deformation regime is typical of transpression (Tikoff and Fossen, 1999; Dewey et al., 1998). In this context is common to observe simultaneously symmetric and asymmetric boudins (Mandal and Karmakar, 1989), as we documented in the studied area. This deformation regime it is compatible also with stress/strain conditions related to the forced intrusion of a plutonic body (see below). The movement direction, reconstructed by analyzing the simple shear kinematic indicators (e.g. asymmetric boudins, mantled porphyroclast, S-C structures), and the asymmetries of the folds (e.g. sheath folds, similar recumbent folds), appears to be preferentially top-to-the-SE, that is consistent with the discharge processes from the flanks of the rising plutonic body.

Structures related to conditions of pure shear are represented by boudinage with neck-type folds and pods of various nature (meta cherts, metapelites and metabasalts) that are characterized by elliptical shape with the main axis parallel to the mylonitic foliation. Given the high variability of the deformations, the kinematic vorticity analysis (PHD and RGN methods) has been applied, in order to quantify the contribution of both simple and pure shear in the mylonitic zone. The two methods gave a 0.70 average value of Wm (with pure and simple shear equally distributed) at both the meso- and microscale. Considering a standard error in the order of 10% (Forte and Bailey, 2007; Zhang et al., 2009), the obtained Wm is entirely in the field of general shear (Fig. 9c; cfr. Forte and Bailey, 2007), confirming the other micro- and meso-structural data. This shear regime is linked to the interaction between intrusion of the plutonic body and host rocks that produced ductile, locally mylonitic deformations in the latter (Fig. 13; see also Lister and Baldwin, 1993; Daniel and Jolivet, 1995; Cifelli et al., 2012). Accordingly, the D_2 structures observed in the contact aureole can be related to a combination of the upward stress, due to the emplacement of the pluton in a pure shear regime, and the lateral ductile flow of PFU in a mainly simple shear regime. These processes allowed also to generate enough space for the intrusion and ballooning of the magmatic body (see also Cifelli et al., 2012).

The magmatic flow structures in the pluton (see Tale 1 in Boccaletti and Papini, 1989), that are coaxial with the Ams lineations of both the magmatic stock and in the PFU rocks (Bouillin et al., 1993, Cifelli et al., 2012) and with the syn-metamorphic stretching lineation and foliations in the latter (Cifelli et al., 2012), together with the petrographic-structural data obtained in the metamorphic aureole (e.g. Wm values), support that most deformations in the metamorphic aureole were not only caused by gravity tectonics, as claimed by the old Authors (e.g. Trevisan 1951), but are strongly related to the hot emplacement of the pluton (see also Daniel and Jolivet, 1995; Cifelli et al., 2012). The development of mylonitic horizons in the carbonate lithologies can be also have been facilitated by a local increases in permeability due to hydrofracturing (see Rossetti et al., 2007), with consequent increase in the circulation of metasomatic fluids. The ductile shear zones can further evolve into brittle-ductile extensional shear zones and allow formation of listric normal fault systems within the sedimentary covers (see following D_3 event) as also suggested in the rheological model of Caggianelli et al. (2013).

D3 event is characterized by non-metamorphic, open to closed folds that deform the F_2 structures (including the mylonitic shear zones) at a metric to decametric scale. Their hinges are always curved and their axial planes have either a low angle or sub-horizontal attitude. The F_3 axial plane foliations are represented by zonal crenulations or fracture cleavage (locally filled with hydrothermal mineralizations). The areal distribution of the F_3 axes is not so different with respect to those of F_2 (Fig. 5), suggesting that the discharge phenomena within the aureole continue from ductile to semi-ductile/semi-brittle conditions, through cascade-type folds (Bouillin, 1983, Coli and Pandeli, 2001), whose axes have an overall tangential distribution with respect to the uprising pluton. During the D_3 event, high angle jointing also occurred in both the pluton and in its contact aureole. These jointing can be related to the last cooling phases and semi-brittle unroofing of the pluton.The comparison with the structural map of the Mt. Capanne pluton in Boccaletti and Papini (1989) shows that the main systems of fractures, that we surveyed in different part of the metamorphic aureole, are mostly parallel to the lineations (longitudinal and cross joints) of the monzogranite (Fig [illegible]). These latter were utilized for the intrusion of the later Orano Porphyry and of the Sant'Ilario Leucogranite, as outlined by previous Authors (Dini et al., 2008b; Principi et al., 2015a). The same results were obtained in the two typical study areas of Colle Palombaia and San Piero (Fig. [illegible]). It is interesting to note the different main orientations of the joints observed in the pluton and in the metamorphic cover in the Colle Palombaia area. In particular, radial-type fractures prevail in the plutonic rocks while tangential-type fractures prevail in the recrystallized cover rocks. Given that the primary intrusive contact is preserved in the Colle Palombaia-Cavoli area, these anomalies could be explained by a different brittle behaviour of the massive monzogranitic rocks respect to the bedded rocks of the metasedimentary cover rather than their growth in different times or during the detachments that locally occurred within the aureole. Also the brittle detachments in the aureole (e.g. CEF, Fetovaia Fault, doublings or remobilization of the ophiolitic sub-units, striated surfaces at the top of the pluton and in the surrounding leucogranites) began and took place during this stage.

D4 event is represented by high angle faulting. In particular, the Colle Palombaia-Procchio high-angle fault (EBF in Figs. 1 and 2) is the main extensional structure in western Elba that downthrows towards the East CU and likely the underlying CEF detachment fault with respect to the PFU hornfels. This structure, that likely contribute to the uplift of the plutonic body and to the erosion of its cover rocks, can be considered as coeval with the N-S and NE-SW normal faults that are more widely developed in Eastern Elba.

Deformation and metamorphic evolution model of western Elba

Taking into account the geological, petrographical-chemical and structural data collected in the metamorphic aureole of the Mt. Capanne pluton, the following sequence of events can be outlined:

1. Deformation and stacking of the Ligurian, Ligurian-Piedmontese and Tuscan tectonic units during the Oligocene to Serravallian syn-collisional shortenings events and readjustment of the nappe pile through low-angle faulting due to the beginning of extensional processes in the inner part of the chain (Fazzuoli et al., 1994; Principi et al., 2015b).

2. The following regional, mainly NW-SE and NS, high-angle normal faulting and associated SW-NE striking transfer shear zones (Bertini et al., 1991; Bartole et al., 1991; Bartole, 1995; Carmignani et al., 1995) produced at times the pathways for the ascent of magmas in the Tuscan Archipelago ("Elba transfer zone" in Dini et al., 2008b) and onland untill Quaternary times (i.e. the Mt. Amiata volcano in Gianelli et al., 1988). In particular, we think that the prolonged activity of the Elba transfer zone (in probable connection with the so-called Piombino-Faenza Line onland) allowed the emplacement of several magmatic bodies in different part of the island. In particular:

a) in Late Tortonian aplitic and porphyritic dikes and laccoliths (Capo Bianco Aplites, Portoferraio and San Martino porphyries) were emplaced in the PFU, EU and CU of western Elba;

b) Forced intrusion and ballooning of the Mt. Capanne pluton occurred (about 6.9 Ma) in the PFU rocks that suffered syn- and post-kinematic contact metamorphism of various grade (D_2 event) (Fig. 13). During this event, folding due to ductile vertical flattening and lateral shearing (e.g. occurrence of mylonitic shear zones) affected the PFU;

c) A mainly radial and tangential jointing event affected the pluton and host metamorphic rocks and was locally sealed by the Orano Porphyry dykes (6.85 Ma) (Dini et al., 2008b), Sant'Ilario Leucogranites and pegmatite, and by the later hydrothermal mineralizations. The uplift of the cooled pluton continued within a semi-ductile/semi-brittle behaviour allowing the cascade-type refolding of PFU (tangentially with respect to the magmatic dome) and enucleation of low- to middle-angle detachment faults in the PFU and in the overlying non-metamorphic Ligurian Units (PTU and EU + CU), producing the west-vergent FF and east-vergent CEF Faults respectivelly (Fig. 14a);

d) Intrusion and unroofing of the 5.9-6.2 Ma Porto Azzurro Monzogranite and dike swarms and formation of Mag-skarn bodies occurred in eastern Elba. Later, the 5.8 Ma mafic Mt. Castello dyke was emplaced and the ZUC and REC detachment faults developed (see Principi et al., 2015a; 2015b) (Fig. 14b).

3. Close to the Miocene-Pliocene boundary, mainly NNE-SSW and NS high-angle normal faults finally cut the whole Elba Island, causing the opening of the Piombino Channel (Fig. 14c); these faults are sealed by 5.4 Ma hematite-rich mineralization in the Porto Azzurro-Cavo area (Lippolt et al., 1995). In western Elba, the Colle Palombaia-Procchio Fault developed on the eastern side of the Mt. Capanne dome, downthrowning towards the East the CU, the underlying EU and PTU and the basal CEF, with respect to the hornfels of the PFU. This process probably helped the plutonic mass to reach its present considerable elevation (1019 m a.s.l).

CONCLUSIVE REMARKS

This study of the contact aureole of the Mt. Capanne pluton allowed to obtain the following main results:

1- The lack of HP-LT minerals within the analyzed rocks (also in the lower contact metamorphic grade) makes it difficult to correlate the PFU rocks with the *Schistes Lustrés* of Alpine Corsica. In spite of the apparent lack of the Nisportino Fm.-like protoliths in the above said hornfels, their correlation with either some of the OU sub-units of Eastern Elba (e.g. Volterraio, Sassi Turchini, Monte Serra and Acquaviva sub-Units) or, more in general, with the Vara Unit seems more suitable.

2- The petrographic and microstructural analyses allowed to define for the first time the metamorphic zonography of the whole aureole. The hornfels are mostly in the medium to high grade facies (Hbl and Py hornfels facies), with T peak > 610°C (perhaps locally > 650°C). Local variations of the zoning are due to the different lithological, physical and structural (e.g. bedding, fracturing) properties of the original rocks, but also to hydrofracturing during syn-metamorphic flow of the metasomatic hot fluids. The growth of the thermometamorphic minerals occurred in several stages, being syn-kinematic with respect to the D_2 folding event up to static post-kinematic.

3- The thickness of the thermometamorphic aureole is estimated in at least 150-200 m.

4- Most of the deformation events in PFU can be related to the dynamic of the Mt. Capanne pluton intrusion and to its unroofing.

5- The D_2 ductile folding and shearing event is related to the intrusion and ballooning of the Mt. Capanne pluton, that caused syn-cinematic deformations parallel to the pluton boundaries in the PFU host Ligurian succession under recrystallization. Our studies define the presence of syn-D_2 mylonites and ultramylonites, never documented up to now in the contact aureole of the Mt. Capanne pluton. The analysis of kinematic indicators and kinematic vorticity in the mylonitic shear zone of the Cavoli-Colle Palombaia area reveals

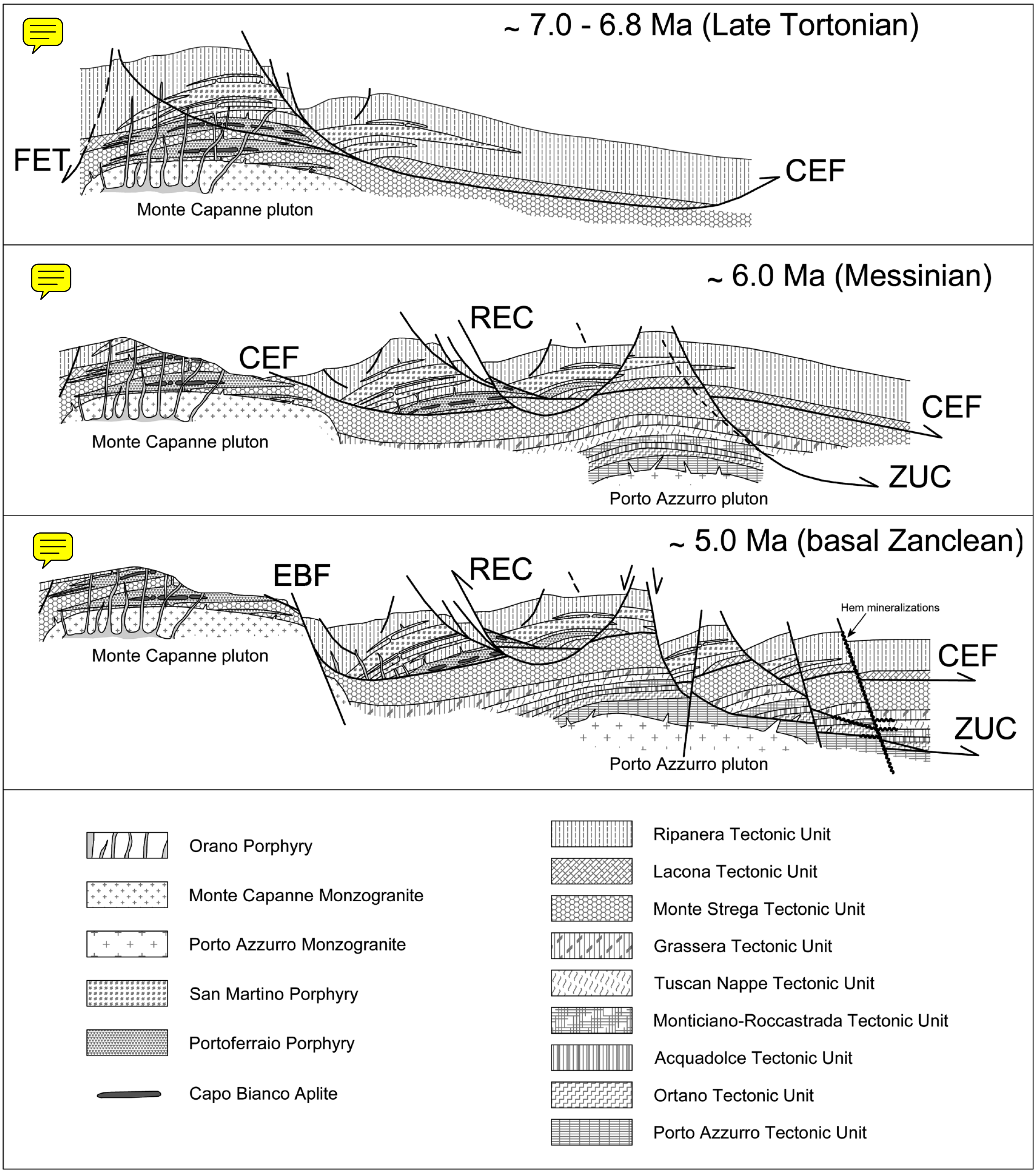

Fig. 14 - Sketch of the geological evolution of the Elba Island from about 7 to 5 Ma (late Tortonian-Present): A- unroofing of the Mt. Capanne pluton and the development of low-angle normal faults, causing westwards (FET- Fetovaia Fault) and eastwards (CEF- Central Elba Fault) delaminations in the tectonic stack. B- Final exhumation of the Porto Azzurro pluton and development of divergent delaminations, westwards (REC- Colle Reciso Fault) and eastward (Zuccale Fault). C- Development of high-angle normal faults (e.g. EBF-Eastern Border Fault) and their filling with Hem-rich mineralizations (modified from Maineri et al., 2003 and Principi et al., 2015b).

the occurrence of a general shear regime during D_2 with a similar distribution of pure and simple shear components (average value of $W_m = 0.7$). This deformation regime can be related to a combination of the vertical uplift of the pluton (pure shear) with the lateral discharge of the covers (simple shear).

6- This multidisciplinary study refines the geological evolution of western Elba Island and show an example of the deformation-metamorphic evolution of a contact metamorphic aureole during a "forced"-type intrusion of a plutonic body.

ACKNOWLEDGMENTS

We are grateful to the Referees (Prof. F.Rossetti of Roma 3 University and an anonymous Referee) for their comments and criticism that significantly improve the original version of this manuscript.

The research was supported by funds of the 1:50,000 scale and 1:25,000 scale maps of the Elba Island for the CARG PROJECT of ISPRA-National Geological Survey of Italy (Coordinator Prof. E. Pandeli) and of the University of Florence.

APPENDIX

X-ray diffraction (XRD) mineralogic analyses were made using a PW 3710 PHILIPS diffractometer (with a anticathode copper tube and graphite filter. The interval 2θ was explored between 5° and 70°, with a speed of goniometer of 2°/minute. The feeding of the tube is 20 mA with a potential of acceleration of 40 kV) at the Earth Sciences Department of the Florence University.

Mineral chemistry data (EMPA) were acquired using a JEOL JXA-8600 electron microprobe (15 kV accelerating voltage, 10 nA beam current) at C.N.R.-I.G.G., Florence, using peak and background counting times of 15 s (10 s for Na) and 5 s, respectively. The data, acquired through XMas software, were corrected using the PAP matrix correction. bdl = below detection limit, blank cells: not analysed.

Recalculations of the EMPA data were performed through the semi-automatic program of the microprobe and spreadsheets for the different mineralogical families (Morimoto et al., 1988 for pyroxene; Rickwood, 1968 for Grts; Rieder et al., 1998 for micas).

REFERENCES

Armbruster T., Bonazzi P., Akasaka M., Bermanec V., Chopin C., Gieré R., Heuss-Assbichler S., Liebscher A., Menchetti S., Pan Y. and Pasero M., 2006. Recommended nomenclature of epidote-group minerals. Eur. J. Miner., 18 (5): 551-567.

Balestrieri M.L., Pandeli E., Bigazzi G., Carosi R. and Montomoli C., 2011. Age and temperature constraints on metamorphism and exhumation of the syn-orogenic metamorphic complexes of Northern Apennines, Italy. Tectonophysics, 509: 254-271.

Barberi F. and Innocenti F., 1965. Le rocce cornubianitico-calcaree dell'anello termometamorfico del Monte Capanne (Isola d'Elba). Atti Soc. Tosc. Sci. Nat. Mem., Ser A, 72: 306-398.

Barberi F. and Innocenti F., 1966. I fenomeni di metamorfismo termico nelle rocce peridotitico serpentinose dell'aureola del Monte Capanne (Isola d'Elba). Per. Miner., 25: 735-768.

Barberi F., Brandi G.P., Giglia G., Innocenti F., Marinelli G., Raggi G., Ricci C.A., Squarci P., Taffi L. and Trevisan L., 1969a. Isola d'Elba, Foglio 126. Carta Geologica d'Italia alla scala 1:100.000, Serv. Geol. d'It., E.I.R.A., Firenze.

Barberi F., Dallan L., Franzini M., Giglia G., Innocenti F., Marinelli G., Raggi R., Squarci P., Taffi L. and Trevisan L. 1969b. Note illustrative della Carta Geologica d'Italia alla scala 1:100.000. Foglio 126 (Isola d'Elba). Serv Geol d'It., 32 pp.

Barboni M. and Schoene B., 2014. Short eruption window revealed by absolute crystal growth rates in a granitic magma. Nature Geosci., 7: 524-528.

Bartole R., 1995. The North Tyrrhenian-Northern Apennines post-collisional system: constraints for a geodynamic model. Terra Nova, 7: 7-30

Bartole R., Torelli L., Mattei G., Peis B. and Brancolin, G., 1991. Assetto stratigrafico-strutturale del Tirreno Settentrionale: stato dell'arte. Studi Geol. Camerti, Vol. Spec. 1991/1: 115-140.

Bailey C.M. and Eyster E.L., 2003. General shear deformation in the Pinaleno Mountains metamorphic core complex, Arizona. J. Struct. Geol., 25: 1883-1893.

Bertini, G., Cameli G.M., Costantini A., Decandia F.A., Di Filippo M., Dini I., Elter M., Lazzarotto A., Liotta D., Pandeli E., Sandrelli F. and Toro B., 1991. Struttura geologica fra i monti di Campiglia e Rapolano Terme (Toscana Meridionale). Stato attuale delle conoscenze e problematiche. Studi Geol. Camerti, Vol. Spec. 1991/1: 155-178.

Bertini G., Gianelli G., Pandeli E. and Puxeddu M., 1985. Distribution of hydrothermal minerals in the Larderello-Travale and Mt. Amiata geothermal fields (Italy). In: Trans. 1985 Intern. Symp. Geothermal energy held in Kailua-Kona (Hawaii), 26-30 August 1985. Geothermal Resources Council, Davis (USA), 9 (1): 261-266.

Bianco C., Brogi A., Caggianelli A., Giorgetti G., Liotta D. snd Meccheri M., 2015. HP-LT metamorphism in Elba Island: Implications for the geodynamicevolution of the inner Northern Apennines (Italy). J. Geodyn., 91: 13-25.

Boccaletti M. and Papini P., 1989. Ricerche meso e microstrutturali sui corpi ignei neogenici della Toscana. 2: L'intrusione del M. Capanne (Isola d'Elba). Boll. Soc. Geol. It., 108: 699-710.

Bortolotti V. and Principi G., 2003. The Bargonasco - Upper Val Graveglia ophiolitic succession, Northern Apennines, Italy. Ofioliti, 28: 137-140.

Bortolotti V., Cellai D., Martin S., Principi G., Tartarotti P. and Vaggelli G., 1994a. Ultramafic rocks from the eastern Elba island ophiolites (Tyrrhenian Sea, Italy). Mem. Soc. Geol. It., 48: 195-202.

Bortolotti V., Fazzuoli M., Pandeli E., Principi G., Babbini A. and Corti S., 2001a. Geology of Central and Eastern Elba Island, Italy. Ofioliti, 26: 97-151.

Bortolotti V., Gardin S., Marcucci M. and Principi G., 1994b The Nisportino Formation: a transitional unit between the Mt. Alpe Cherts and the Calpionella Limestones (Vara Supergroup, Elba Island, Italy). Ofioliti, 19: 349-365.

Bortolotti V., Pandeli E. and Principi G., 2001b. The geology of the Elba Island: an historical introduction. Ofioliti, 26: 79-96.

Bortolotti V., Pandeli E. and Principi G., 2015. Carta geologica dell'Isola d'Elba, Scala 1:25.000. Note illustrative / Geological Map of Elba Island, 1:25,000 Scale. Explanatory notes. D.R.E.A.M., 74 pp.

Bouillin J.P., 1983. Exemples de déformations locales liées à la mise en place de granitoïdes alpins dans des conditions distensives: l'Ile d'Elbe (Italie) et le Cap Bougaroun (Algérie). Rev. Géo. Dyn. Géogr. Phys., 24: 101-116.

Boullin J.P., Bouchez J.L., Lespinasse L. and Pecher A., 1993. Granite emplacement in extensional setting: an AMS study of the magmatic structures of Monte Capanne (Elba, Italy) Earth. Planet. Sci. Lett., 118: 263-269.

Bouillin J.P., Poupeau G. and Sabil N., 1994. Etude thermochronologique de la dénudation du pluton du Monte Capanne (Ile d'Elbe, Italie) par les traces de fission. Bull. Soc. Géol. Fr., 165: 19-25.

Brunet C., Monie P., Jolivet L. and Cadet J.P., 2000. Migration of compression and extension in the Tyrrhenian Sea, insights from $^{40}Ar/^{39}Ar$ ages on micas along a transect from Corsica to Tuscany. Tectonophysics, 321: 127-155.

Buriánek D. and Dolníček Z., 2011. Metamorphic evolution of the contact aureole of the Dipilto Batholith, Eastern Chortis Terrane, Nicaragua. J. Geosci., 56: 9-26.

Burkhard M., 1993. Calcite twins, their geometry, appearance and significance as stress-strain markers and indicators of tectonic regime: a review. J. Struct. Geol., 15: 351-368.

Bucher K. and Frey M., 1994. Petrogenesis of metamorphic rocks. Springer Ed., 6th edition, 318 pp.

Bucher K. and Grapes R., 2011. Petrogenesis of metamorphic rocks. Springer Ed., 8_{th} edition, 428 pp.

Caggianelli A., Ranalli G., Lavecchia A., Liotta D. and Dini A., 2013. Post-emplacement thermo-rheological history of a granite intrusion and surroundings rocks: the Monte Capanne pluton, Elba Island, Italy. In: S. Llana-Fùnez., A. Marcos and F. Bastida (Eds.), Deformation structures and processes within the continental crust. Geol. Soc. London Spec. Publ., 394: 129-143.

Carmignani L., Decandia F.A., Disperati L., Fantozzi P.L., Lazzarotto A., Liotta D. and Oggiano G., 1995. Relationship between the Tertiary structural evolution of the Sardinia-Corsica-Provencal Domain and the Northern Apennines. Terra Nova, 7: 128-137.

Casillas R., Demény A., Nagy G., Ahijado A. and Fernández C., 2011. Metacarbonatites in the Basal Complex of Fuerteventura (Canary Islands). The role of fluid/rock interactions during contact metamorphism and anatexis. Lithos, 125: 503-520.

Cifelli F., Minelli L., Rossetti F., Urru G. and Mattei M., 2012. The emplacement of the Late Miocene Monte Capanne intrusion (Elba Island, Central Italy): constraints from magnetic fabric analyses. Intern. J. Earth Sci. (Geol. Rundsch.), 101: 787-802.

Coli M. and Pandeli E., 2001. The Ophiolitic unit of Fetovaia-Pomonte and Punta Nera zone, Western Mt. Capanne thermometamorphic aureola. In: V. Bortolotti (Ed.), Meeting E.L.I.C.A. 97 "The Elba Island: a key puzzle linking the Corso-Sardinian massif and Adria". Pre-meeting transect Corsica - Elba Island - Southern Tuscany. 2- Elba Island. C - Western Elba, a). Excursion Guidebook. Ofioliti 26: 347-350.

Conticelli S., Bortolotti V., Principi G., Laurenzi M.A. D'Antonio M. and Vaggelli G., 2001b. Petrology, mineralogy and geochemistry of a mafic dike from Monte Castello, Elba Island, Italy. Ofioliti 26: 249-262.

Conticelli S., Moratti G., Papini P. and Tommasini S., 2001a. The Monte Capanne monzogranite. In: V. Bortolotti (Ed.), Meeting E.L.I.C.A. 97 "The Elba Island: a key puzzle linking the Corso-Sardinian massif and Adria". Pre-meeting transect Corsica - Elba Island - Southern Tuscany. 2 - Elba Island. C - Western Elba, b). Excursion Guidebook. Ofioliti 26: 350-356.

Corsi B., Elter F.M., Pandeli E. and Sandrelli F., 2001. Caratteri strutturali del Gruppo del Verrucano (Unità di Monticiano-Roccastrada) nella Toscana Meridionale ed insulare. Atti Ticin. Sci. Terra, Pavia, 42: 47-58.

Cortesogno L., Galbiati B. and Principi G., 1987. Note alla "Carta geologica delle ofioliti del Bracco" e ricostruzione della paleogeografia Giurassico-Cretacica. Ofioliti, 12: 261-342.

Cortesogno L., Gianelli G. and Piccardo G., 1975. Preorogenic metamorphic and tectonic evolution of the ophiolite mafic rocks (northern Apennine and Tuscany). Boll. Soc. Geol. It., 94: 291-327.

Costamagna L.G., Elter F.M., Gaggero L. and Mantovani F., 2016. Contact metamorphism in middle-Ordovician rocks (SW Sardinia, Italy): new paleogeographic constraints. Lithos, 264: 577-593.

Daniel J.M. and Jolivet L. 1995. Detachment faults and pluton emplacement: Elba Island (Tyrrhenian Sea). Bull. Soc. Géol. Fr., 166: 341-354.

De Paor D.G., 1988. Rf/Øf strain analysis using an orientation net. J. Struct. Geol., 10: 323-333.

Deino A., Keller J.V.A., Minelli G., and Pialli G., 1992. Datazioni $^{40}Ar/^{39}Ar$ del metamorfismo dell'Unità di Ortano-Rio Marina (Isola d'Elba): risultati preliminari. Studi Geol Camerti, Vol. Spec. 1992/2: 187-192.

Dewey J.F., Holdsworth R.E. and Strachan R.A., 1998. Transpression and transtension zones. Geol. Soc. London Spec. Publ., 135 (1): 1-14.

Dini A., Farina F., Innocenti F., Rocchi S. and Westerman D.S., 2007. Monte Capanne Pluton revisited 40 years after Giglia's contributions. Rend. Soc. Geol. It., 5: 126-128.

Dini A., Innocenti F., Rocchi S., Tonarini S. and Westerman D.S., 2002. The magmatic evolution of the Upper Miocene laccolith-pluton-dyke granitic complex of Elba Island, Italy. Geol. Mag. 139: 257-279.

Dini A., Mazzarini F., Musumeci G. and Rocchi S., 2008a. Multiple hydro-fracturing by boron-rich fluids in the Upper Miocene contact aureole of eastern Elba Island (Tuscany, Italy). Terra Nova, 20: 318-332,

Dini A., Rocchi S., Westerman D.S. and Farina F., 2009. The Upper Miocene intrusive complex of Elba Island: two centuries of studies from Savi to Innocenti. In: P. Armienti, M. D'Orazio and S. Rocchi (Eds.), A volume dedicated to Professor Fabrizio Innocenti. Acta Vulcan., 20-21: 11-32.

Dini A., Westerman D.S., Innocenti F. and Rocchi S., 2008b. Magma emplacement in a transfer zone: the Miocene mafic Orano dike swarm of Elba Island (Tuscany), In: K. Thomson and N. Petford (Eds.), Structure and emplacement of High-Level Magmatic Systems. Geol. Soc., London Spec. Publ., 302: 131-148.

Durand Delga M., 1984. Principaux traits de la Corse alpine et corrélations avec les Alpes ligures. Mem. Soc. Geol. It., 28: 185-329.

Durand-Delga M., 1978. La Corse. Guide géologiques régionaux. Masson, Paris, 208 pp.

Duranti S., Palmeri R., Pertusati P.C. and Ricci C.A., 1992. Geological evolution and metamorphic petrology of the basal sequences of Eastern Elba (Complex II). Acta Vulcan., 2: 213-229.

El Khalile A., Touil A., Hibti M. and Bilal E., 2014. Metasomatic zoning, mineralizations and genesis of Cu, Zn and Mo Azegour skarns (western high Atlas, Morocco). Carpath. J. Earth Envir. [illegible] 9 (1): 21-32.

Elter F.M. and Pandeli E., 2002. The HP-LP meta-ophiolitic unit and Verrucano of the Cala Grande area in the Argentario Promontory (Southern Tuscany, Italy): structural-metamorphic evolution and regional considerations. Ofioliti, 27: 91-102.

Elter F.M. and Sandrelli F., 1995. La Fase Post Nappe nella Toscana Meridionale: considerazioni sull'evoluzione dell'Appennino Settentrionale. In: Geodinamica e tettonica attiva del sistema Tirreno - Appennino. Atti Ticin. Sci. Terra, Pavia, 37: 173-193.

Farina F., Dini A., Innocenti F., Rocchi S. and Westerman D.S., 2010. Rapid incremental assembly of the Monte Capanne pluton (Elba Island, Tuscany) by downward stacking of magma sheets. Geol. Soc. Am. Bull., 122: 1463-1479.

Fazzuoli M., Pandeli E. and Sani F., 1994. Considerations on the sedimentary and structural evolution of the Tuscan Domain since Early Liassic to Tortonian. Mem. Soc. Geol. It., 48: 31-50.

Ferrara G. and Tonarini S., 1985. Radiometric geochronology in Tuscany: results and problems. Rend. Soc. It.. Miner. Petr., 40: 111-124.

Ferrara G. and Tonarini S., 1993. L'Isola d'Elba: un laboratorio di geocronologia. Mem. Soc. Geol. It., 49: 227-232.

Ferrill D.A., Morris A.P., Evans M.A., Burkhard M., Groshong R.H. and Onasch C.M. 2004. Calcite twin morphology: a low temperature deformation geothermometer. J. Struct. Geol., 26 (8): 1521-1529.

Forte A.M. and Bailey C.M. 2007. Testing the utility of the porphyroclast hyperbolic distribution method of kinematic vorticity analysis. J. Struct. Geol., 29: 983-1001.

Gagnevin D., Daly J. and Poli G., 2004. Petrographic, geochemical and isotopic constraints on magma dynamics and mixing in the Miocene Monte Capanne monzogranite (Elba Island, Italy). Lithos, 78: 157-195.

Gagnevin D., Daly J. and Poli G., 2008. Insights into granite petrogenesis from quantitative assessment of the field distribution of enclaves, xenoliths and K-feldspar megacrysts in the Monte Capanne pluton, Italy. Miner. Mag., 72: 925-940.

Garfagnoli F., Menna, F., Pandeli E. and Principi G., 2005. The Porto Azzurro Unit (Mt. Calamita Promontory, southeastern Elba Island, Tuscany): stratigraphic, tectonic and metamorphic evolution. Boll. Soc. Geol. It., Vol. Spec. 3: 119-138.

Gianelli, G., Puxeddu, M., Batini, F., Bertini, G., Dini, I., Pandeli, E. and Nicolich, R., 1988. Geological model of a joung volcano-plutonic system: the geothermal region of Monte Amiata (Tuscany, Italy). Geothermics, 17: 719-734.

Jessup M.J., Law R.D. and Frassi C., 2007. The Rigid Grain Net

(RGN): An alternative method for estimating mean kinematic vorticity number (Wm). J. Struct. Geol. 29: 411-421.

Johnson T.E., Hudson N.F.C. and Droop G.T.R., 2000. Wollastonite-bearing assemblages from the Dalradian at Fraserburgh, northeast Scotland and their bearing on the emplacement of garnetiferous granitoid sheets. Miner. Mag., 64: 1165-1176.

Jolivet L., Faccenna C., Goffé B., Mattei M., Rossetti F., Brunet C., Storti F., Funiciello R., Cadet J.P., D'Agostino N. and Parra T., 1998. Midcrustal shear zones in postorogenic extension: example from the northern Tyrrhenian Sea. J. Geophys. Res., 103 (B6): 12123-12160.

Juteau M., Michard A., Zimmermann J.L. and Albarede F., 1984. Isotopic heterogeneities in the granitic intrusion of Monte Capanne (Elba Island, Italy) and dating concepts. J. Petrol., 25: 532-545.

Keller J.V.A. and Pialli G., 1990. Tectonics of the Island of Elba: a reappraisal. Boll. Soc. Geol. It., 109: 413-425.

Kerrick D.M., 1991. Overview of contact metamorphism. Rev. Miner. Geochem., 2 (1): 1-12.

Klepeis K.A., Daczko N.R. and Clarke G.L., 1999. Kinematic vorticity and tectonic significance of superposed mylonites in a major lower crustal shear zone, northern Fiordland, New Zealand. J. Struct. Geol., 21: 1385-1406.

Law R.D., Searl, M.P. and Simpson R.L., 2004. Strain, deformation temperatures and vorticity of flow at the top of the Greater Himalayan Slab, Everest Massif, Tibet. J. Geol. Soc. London, 161: 305-320.

Leake B.E., 1978. Nomenclature of amphiboles. Can. Miner., 16: 501-520.

Lippolt H.J., Wernicke R.S. and Bähr R., 1995. Paragenetic specularite and adularia, Elba Island, Italy: Concordant, U+Th-He and K-Ar ages. Earth Planet. Sci. Lett., 132: 43-51.

Lister G.S. and Baldwin S.L., 1993. Plutonism and the origin of metamorphic core complexes. Geology, 21: 607-610.

Maineri C., Benvenuti M., Costagliola P., Dini A., Lattanzi P., Ruggieri G. and Villa I.M., 2003. Sericitic alteration at the La Crocetta deposits (Elba Island, Italy): interplay between magmatism, tectonic and hydrothermal activity. Miner. Dep., 38: 67-86.

Mandal N. and Karmakar S., 1989. Boudinage in homogeneous foliated rocks. Tectonophysics, 170: 151-158.

Marinelli G., 1959. Le intrusioni terziarie dell'Isola d'Elba. Atti Soc. Tosc. Sci. Nat. Mem. Ser A, 66: 50-223

Marroni M., Bortolotti V., Cortesogno L., Gaggero L., Lahondere D., Molli G., Montanini A., Pandolfi L., Principi G., Rossi P., Saccani E., Treves B. and Tribuzio R., 2004. Northern Apennine and Corsican ophiolites: the oceanic lithosphere of the Ligure-Piemontese basin and its transition to the Adria continental margin (Italy). In: L. Guerrieri, I. Rischia and L Serva (Eds.). - Excursion Guidebook of the "32nd International Geological Congress ITALIA 2004". Volume n° 4 (from P14 to P36), P 27 Post-Congress Field Trip Guide. Apat, Roma: 52 pp.

Massa G., Musumeci G., Mazzarini F. and Pieruccioni D., 2016. Coexistence of contractional and extensional tectonics during the northern Apennines orogeny: the late Miocene out-of-sequence thrust in the Elba Island nappe stack. Geol. J., 2016.

Molli G., 2008. Northern Apennine-Corsica orogenic system: an updated review. Geol. Soc. London Spec. Publ., 298: 413-442.

Morimoto N., 1988. Nomenclature of pyroxene. Miner. Petrol., 39: 55-76.

Musumeci G., Mazzarini F., Tiepolo M. and Di Vincenzo G., 2010. U-Pb an ^{40}Ar-^{39}Ar geochronology of Paleozoic units in the northern Apennines: determining protolith age and alpine evolution using the Calamita Schists and Ortano Porphyroid. Geol. J., 45: 1-23.

Nirta G., Pandeli E., Principi G., Bertini G. and Cipriani N., 2005. The Ligurian Units of Southern Tuscany. Boll. Soc. Geol. It.,Vol. Spec. 3: 29-54.

Orlandi P. and Pezzotta F., 1997. Minerali dell'Isola d'Elba, i minerali dei giacimenti metalliferi dell'Elba orientale e delle pegmatiti del M. Capanne. Ed. Novecento Grafico, Bergamo, 245 pp.

Orlandi P., Pasero M. and Perchiazzi N., 1990. Nb-Ta oxides from Elba Island pegmatites. Atti Soc. Tosc. Sci. Nat. Mem. Ser. A, 97: 161-173.

Orti L., Morelli M., Pandeli E. and Principi G., 2002. New geological data from Gorgona Island (Northern Tyrrhenian Sea). Ofioliti, 27: 133-144.

Pandeli E., Corti S., Franceschelli M. and Pecchioni E., 2001b. The varicoloured slates of the Gràssera Unit (Central-Eastern Elba, Tuscany): petrographical-mineralogical data and comparisons with other Tuscan and Ligurian-Piedmontese units. Ofioliti, 26: 197-206.

Pandeli E., Principi G., Bortolotti V., Benvenuti M., Fazzuoli M., Dini A., Fanucci F., Menna F. and Nirta G., 2013. The Elba Island: an intriguing geological puzzle in the Northern Tyrrhenian Sea. ISPRA and Soc. Geol. It., Geol. Field Trips, Vol. 5 No. 2.1, SGI: 114 pp.

Pandeli E., Puxeddu M. and Ruggieri G., 2001a. The metasiliciclastic-carbonate sequence of the Acquadolce Unit (Eastern Elba Island): new petrographic data and paleogeographic interpretation. Ofioliti, 26: 207-218.

Pandeli E., Santo A.P., Candido M.R., Petrone C.M. and Giusti R., 2014. The calc-alkaline Monte Capo Stella dykes in the Ophiolitic Unit of the Elba Island (Italy): geological setting and compositional characterization. Ofioliti, 39: 79-93.

Pandeli E., Santo A.P., Morelli M. and Orti L., 2006. Petrological and geological data of porphyritic dykes from the Capo Arco area (eastern Elba island, northern Tyrrhenian sea). Per. Miner., 75: 291-302.

Passchier C.W. and Trouw R.A.J., 1996. Microtectonics. Springer Verlag, Berlin, 289 pp.

Perrin M., 1975. L'Ile d'Elbe et la limite Alpes-Apennin: données sur la structure géologique et l'évolution tectogénétique de l'Elbe alpine et de l'Elbe apennine. Boll. Soc. Geol. It., 94: 1929-1955.

Pertusati P.C., Raggi C., Ricci C.A., Duranti S. and Palmeri R., 1993. Evoluzione post-collisionale dell'Elba centro-orientale. Mem. Soc. Geol. It., 49: 223-312.

Pezzotta F., 2000. Internal structures, parageneses and classification of the miarolitic Li-bearing complex pegmatites of Elba Island (Italy). Mem. Soc. It. Sci. Nat., Museo Civico Storia Nat. Milano, 30: 29-43.

Poli G., 1992. Geochemistry of Tuscan Archypelago granitoids, Central Italy: the role of hybridization and accessory phases crystallization in their genesis. J. Geol., 100: 41-56.

Poli G. and Peccerillo A., 2016. The Upper Miocene magmatism of the Island of Elba (Central Italy): compositional characteristics, petrogenesis and implications for the origin of the TuscanyMagmatic Province. Miner. Petrol., 110 (4): 421-445.

Principi G., Bortolotti V., Pandeli E. et al., 2015a. Carta geologica d'Italia alla scala 1:50.000 Foglio 316, 317, 328, 329 Isola d'Elba - Geological Map of Italy at 1:50.000 scale, Sheet Isola d'Elba. ISPRA - Serv. Geol. d'It., Selca, Firenze and Dream, Pratovecchio (AR).

Principi G., Bortolotti V., Pandeli E., Benvenuti M., Fanucci F., Chiari M., Dini A., Fazzuoli M., Menna F., Moretti S., Nirta G. and Reale V., 2015b. Note illustrative della Carta Geologica d'Italia alla scala 1:50.000, Foglio 316, 317, 328, 329 Isola d'Elba. ISPRA Serv. Geol. d'It,, Roma and Selca, Firenze, 263 pp.

Principi G., Bortolotti V., Pandeli E. et al., 2015c. Carta Geologica dell'Isola d'Elba alla scala 1:25.000 - Geological Map of the Elba Island at 1:25,000 scale. D.R.E.A.M., Pratovecchio (AR).

Ramsay J.G., 1967. Folding and fracturing of rocks. McGraw-Hill, New York, 568 pp

Reutter K.J. and Spohn A., 1982. The position of the West-Elba ophiolites within the tectonic framework of the Apennines. Ofioliti, 7: 467-478.

Rieder M., Cavazzini G., D'yakonov Y.S., Frank-Kamenetskii V.A., Gottardi G., Guggenhein S., Koval P.V. and Wones D.R., 1998. Nomenclature of the micas. Can. Miner., 36 (3): 905-912.

Rocchi S., Dini A., Innocenti F., Tonarini S. and Westerman D.S.,

2003. Elba Island: intrusive magmatism. Periodico di Mineralogia, 72 (2): 73-104.

Rocchi S., Westerman, D.S., Dini A., Innocenti F. and Tonarini S., 2002. Two-stage growth of laccoliths at Elba Island, Italy. Geology, 30: 983-986.

Rocchi S., Westerman D.S., Dini A. and Farina F., 2010. Intrusive sheets and sheeted intrusions at Elba Island (Italy). Geosphere, 6: 225-236.

Rossetti F. and Tecce F., 2008. Composition and evolution of fluids during skarn development in the Monte Capanne thermal aureole, Elba Island, central Italy. Geofluids, 8: 167-180.

Rossetti F., Faccenna C., Jolivet L., Funiciello R., Tecce F. and Brunet C., 1999. Syn- versus postorogenic extension: the case study of Giglio Island (northern Tyrrhenian Sea, Italy). Tectonophysics, 304: 71-93.

Rossetti F., Faccenna C., Jolivet L., Funiciello R., Goffé B., Tecce F., Brunet C., Monié P. and Vidal O., 2001. Structural signature and exhumation P-T-T path of the Gorgona blueschist sequence (Tuscan Archipelago, Italy). Ofioliti, 26:175-186.

Rossetti F., Tecce F., Billi A. and Brilli M., 2007. Patterns of fluid flow in the contact aureole of the Late Miocene Monte Capanne pluton (Elba Island, Italy): the role of structures and rheology. Contrib. Miner. Petrol., 153: 743-760.

Ruggieri G., Petrone C.M., Gianelli G., Arias A. and Torio Henriquez E., 2006. Hydrothermal alteration in the Berlin geothermal field (El Salvador): new data and discussion on the natural state of the system. Per. Miner., 75 (2-3): 293-312.

Saupé F., Marigna, C., Moine B., Sonet J. and Zimmermann J.L., 1982. Datation par les methods K/Ar et Rb/Sr de quelques roches de la partie orientale de l'Ile d'Elbe (Province de Livourne, Italie). Bull. Miner., 105: 236-245.

Serri G., Innocenti F. and Manetti P., 1993. Geochemical and petrological evidence of the subduction of delaminated Adriatic continental lithosphere in the genesis of the Neogene-Quaternary magmatism of Central Italy. Tectonophysics, 223: 117-147.

Simpson C. and De Paor D.G., 1993. Strain and kinematic analysis in general shear zones. J. Struct. Geol., 15: 1-20.

Spohn A., 1981 Die ophiolitführenden Gesteine von West-Elba: Stratigraphie, Tektonik, Metamorphose. Berliner Geowiss. Abh. Reihe, A 37, 124 pp.

Tanelli G., Benvenuti M., Costagliola P., Dini A., Lattanzi P., Maineri C., Maineri C., Mascaro I. and Ruggieri G., 2001. The iron mineral deposits of Elba Island: state of the art. Ofioliti, 26: 239-248.

Tindle A.G. and Webb P.C., 1994. Probe-Amph - A spreadsheet program to classify microprobe-derived amphibole analyses. Comp. Geosci., 20: 1201-1228.

Tikoff B. and Fossen H., 1999. Three dimensional reference deformations and strain facies. J. Struct. Geol., 21: 1497-1512.

Trevisan L., 1950. L'Elba orientale e la sua tettonica di scivolamento per gravità. Mem. Ist. Geol. Univ. Padova, 16: 5-39.

Trevisan L. 1951. La 55ª Riunione Estiva della Società Geologica Italiana. Isola d'Elba, Settembre 1951. Boll. Soc. Geol. It., 70: 435-472 (1953).

Turner F.J., 1981. Metamorphic petrology - Mineralogical, field and tectonic aspects. 2nd edn. McGraw-Hill, New York, 524 pp.

Westerman D.S., Dini A., Innocenti F. and Rocchi S., 2003. When and where did hybridization occur? The case of the Monte Capanne pluton, Italy. Atlantic Geol., 39:147-162.

Westerman D.S., Dini A., Innocenti F., Rocchi S., 2004. Rise and fall of a nested christmas-tree laccolith complex, Elba Island, Italy. In: N. Petford and C. Breitkreutz (Eds.), Physical geology of high-level magmatic systems. Geol. Soc. London Spec. Publ., 234:195-213.

Whitney D.L. and Evans B.W., 2010. Abbreviations for names of rock-forming minerals. Am. Miner., 95: 185-203.

Winkler H.G.F., 1979. Petrogenesis of metamorphic rocks. 5nd Edition. Springer-Werlag, New York-Heidelberg-Berlin, 348pp.

Winter J.D., 2010. Principles of igneous and metamorphic petrology. 2nd Edition. Pearson, Withman College, 702 pp.

Xypolias P., 2010. Vorticity analysis in shear zones: a review of methods and applications. J. Struct. Geol. 32 (12), 2072-2092.

Xypolias P. and Koukouvelas I.K., 2001. Kinematic vorticity and strain patterns associated with ductile extrusion in the Chelmos shear zone (External Hellenides, Greece). Tectonophysics, 338: 59-77.

Zhang B., Zhang J., Zhong D. and Guo L., 2009. Strain and kinematic vorticity analysis: An indicator for sinistral transpressional strain-partitioning along the Lancangjiang shear zone, western Yunnan, China. Sci. in China Series D: Earth Sci., 52: 602-618.

Received, May 22, 2017
Accepted, September 21, 2017

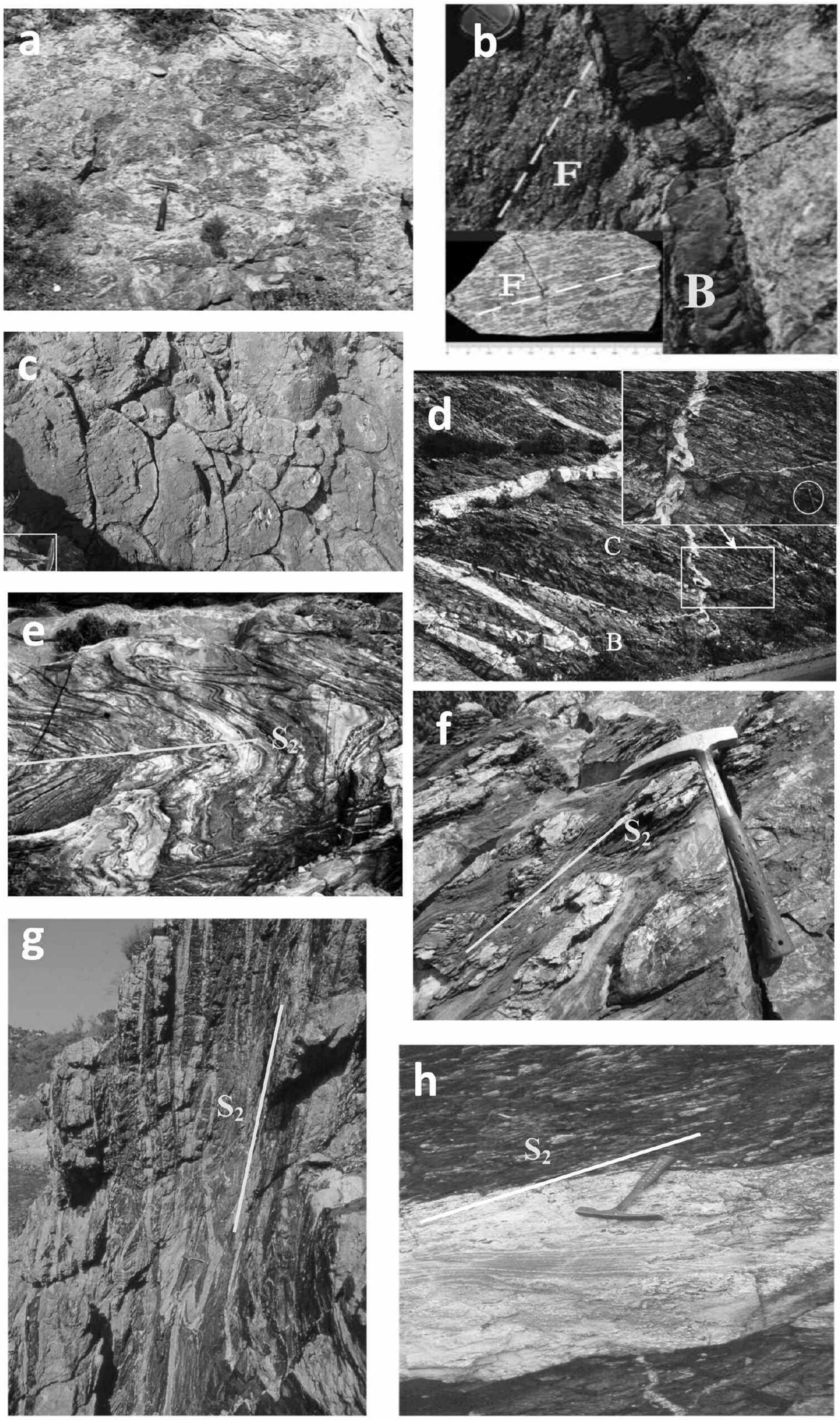

Plate 1 - Outcrops of the formations in the Punta Polveraia-Fetovaia Unit: a) Serpentinites at Colle Palombaia; b) Outcrop of flaser-type metagabbro (F = foliation) cut by an underformed basaltic dike (B) in the Ogliera area (coast south of Pomonte) and polished section of flaser-gabbro; c) Pillow metabasalts at Punta della Crocetta (east of Marciana Marina) (scale = squared hammer); d) Outcrop and closeup of recrystallized blackish metacherts (C) cut by swarms of post-Capanne aplitic dikes (panoramic road south of Pomonte) and basal contact with metabasalts (B) (scale = encircled hammer); e) Folded marbles of the metalimestones at Spartaia (see also Fig. 6) (same scale of Fig.2); f) Folded marbles and calcschists of the metalimestones at Ogliera; g) Metashales with metalimestone intercalations and exoskarns at Punta della Fornace (NW of Colle d'Orano); h) Foliated Portoferraio-type metaporphyritic dike within the metashales and metalimestones at Punta del Timone (panoramic road north of Chiessi).

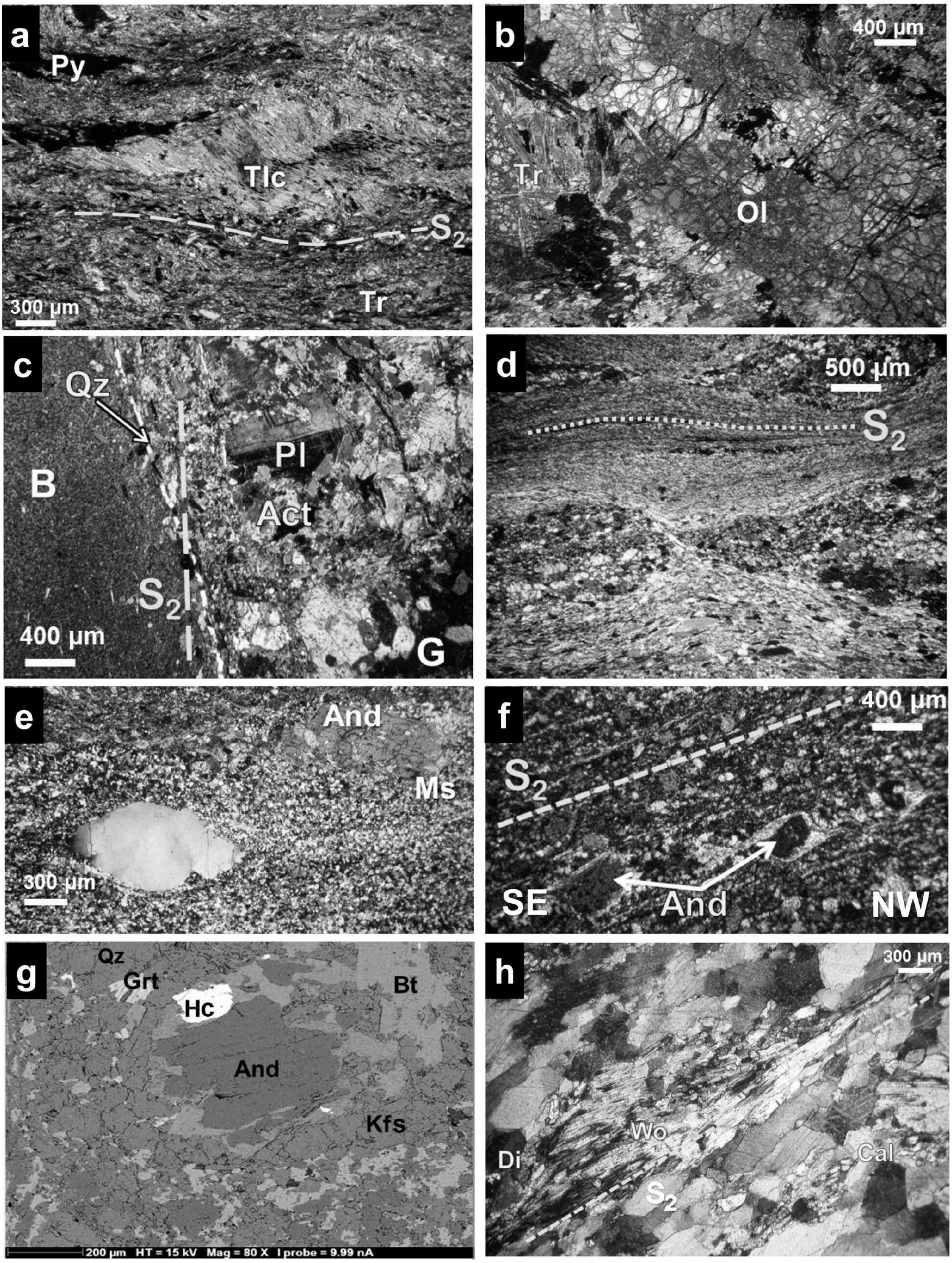

Plate 2 - Photomicrographs of the contact mineralogic assemblages and structures in the rocks of PFU: a) Rotate syn-tectonic Tlc porphyroclast within the main Amp foliation in the serpentinites at Colle Palombaia; b) Neoblastic Ol after cellular Srp in the serpentinites at Punta Nera; c) Foliated contact between metagabbros (G) and metabasalts (B) at Colle Palombaia with a Qz vein; d) Foliated metabasalts at Colle Palombaia; e) Metacherts with And porphyroblasts at Colle Palombaia; f) Mantled And porphyroclasts in the metacherts at Colle Palombaia; g) SEM image of Hc-bearing metacherts at Colle Palombaia; h) Wo and Di lying along the main foliation in the metalimestones at Cavoli-Colle Palombaia; i) Deformed Wo- and Ves-bearing main foliation in the metalimestones at Cavoli-Colle Palombaia; j) Mantled Di porphyroclasts within the main foliation in the exoskarn levels of the metashales and metalimestones at Punta della Fornace (NW of Colle d'Orano); k) Static Wo radiating sphaerule with Di core in the metalimestones at S[illegible]foro locality; l) Wo+Ves in a decarbonated exoskarn of the metalimestones at Cavoli-Colle Palombaia; m) Tur-rich, foliated Portoferraio

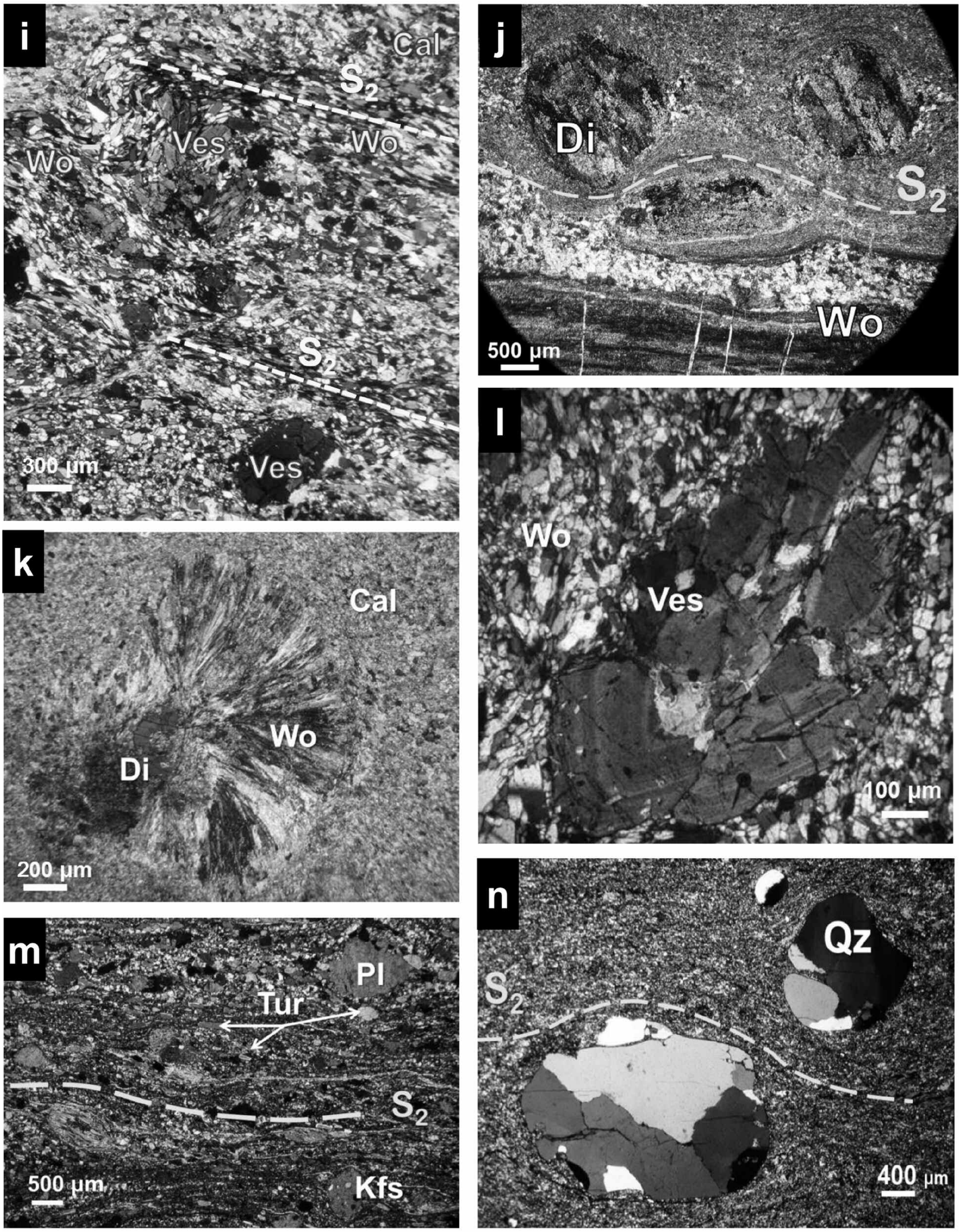
i
Cal
S2
Ves
Wo
Wo
S2
300 μm
Ves
j
Di
S2
Wo
500 μm
k
Cal
Wo
Di
200 μm
l
Wo
Ves
100 μm
m
Pl
Tur
S2
500 μm
Kfs
n
Qz
S2
400 μm